

1-1-2005

Application of computational fluid dynamics on smart wing design

Parthasarathy Chinnasamy
University of Nevada, Las Vegas

Follow this and additional works at: <https://digitalscholarship.unlv.edu/rtds>

Repository Citation

Chinnasamy, Parthasarathy, "Application of computational fluid dynamics on smart wing design" (2005).
UNLV Retrospective Theses & Dissertations. 1823.
<http://dx.doi.org/10.25669/pdti-wjm2>

This Thesis is protected by copyright and/or related rights. It has been brought to you by Digital Scholarship@UNLV with permission from the rights-holder(s). You are free to use this Thesis in any way that is permitted by the copyright and related rights legislation that applies to your use. For other uses you need to obtain permission from the rights-holder(s) directly, unless additional rights are indicated by a Creative Commons license in the record and/or on the work itself.

This Thesis has been accepted for inclusion in UNLV Retrospective Theses & Dissertations by an authorized administrator of Digital Scholarship@UNLV. For more information, please contact digitalscholarship@unlv.edu.

APPLICATION OF COMPUTATIONAL FLUID DYNAMICS ON
SMART WING DESIGN

by

Parthasarathy Chinnasamy

Bachelor of Engineering
SSM College of Engineering, India
2002

A thesis submitted in partial fulfillment
of the requirements for the

Master of Science Degree in Mechanical Engineering
Department of Mechanical Engineering
Howard R. Hughes College of Engineering

Graduate College
University of Nevada, Las Vegas
August 2005

UMI Number: 1429697

INFORMATION TO USERS

The quality of this reproduction is dependent upon the quality of the copy submitted. Broken or indistinct print, colored or poor quality illustrations and photographs, print bleed-through, substandard margins, and improper alignment can adversely affect reproduction.

In the unlikely event that the author did not send a complete manuscript and there are missing pages, these will be noted. Also, if unauthorized copyright material had to be removed, a note will indicate the deletion.

UMI[®]

UMI Microform 1429697

Copyright 2006 by ProQuest Information and Learning Company.

All rights reserved. This microform edition is protected against unauthorized copying under Title 17, United States Code.

ProQuest Information and Learning Company
300 North Zeeb Road
P.O. Box 1346
Ann Arbor, MI 48106-1346



Thesis Approval
The Graduate College
University of Nevada, Las Vegas

June 17, 2005

The Thesis prepared by

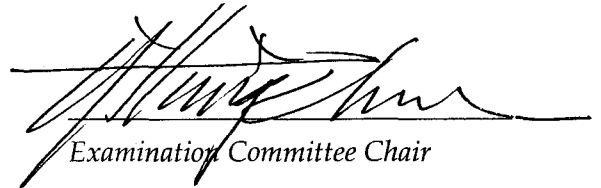
Parthasarathy Chinnasamy


Entitled

Application of Computational Fluid Dynamics on Smart Wing Design

is approved in partial fulfillment of the requirements for the degree of

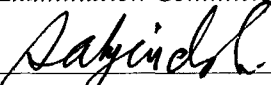
Master of Science Degree in Mechanical Engineering


Examination Committee Chair


Dean of the Graduate College


Examination Committee Member


Examination Committee Member


Graduate College Faculty Representative

ABSTRACT

Application of Computational Fluid Dynamics on Smart Wing Design

by

Parthasarathy Chinnasamy

Dr. Yitung Chen, Examination Committee Chair
Associate Professor, Department of Mechanical Engineering
University of Nevada, Las Vegas

The instantaneous shape of the wing has a profound effect on the fluid dynamic forces it can generate. Visualization of the results obtained from the CFD code gives a better understanding of the happenings around a bending airfoil. The proposed Computational Fluid Dynamics (CFD) model provides detailed design information for the lift and drag forces, velocity and static pressure changes around an airfoil during take off, flying, and landing. Commercial CFD package—FLUENT is used to evaluate the smart material airfoil aerodynamics performance. The results are then compared with the parametric conventional wings—the wings with flaps. Using smart materials the wings can be designed to vary their stiffness with time. A flexible wing is useful to increase lift and reduce drag. A parametric bending profile of a smart flap is designed considering different types of beams. Cantilever beam with uniformly varying load with roller support at the free end is considered here. The bending profile of the above said beam is similar to the bending profile we are about to investigate. Flexible airfoil is designed using the bending equations. The design is then meshed using GAMBIT and exported to

FLUENT. Boundary conditions are defined and CFD modeling is done. One other method is also used for designing the bending flaps. It was named as tangent arc method. The effect of changing pivot point is analyzed since it has considerable impact on aerodynamic performance of smart airfoils. Finally, the assumption made for conventional wings is validated with wind tunnel test data.

TABLE OF CONTENTS

ABSTRACT	iii
LIST OF FIGURES	vii
LIST OF TABLES.....	ix
ACKNOWLEDGMENTS	x
NOMENCLATURE	xi
CHAPTER 1 INTRODUCTION	1
1.1 History of Wings	2
1.2 Smart Wings	3
1.3 Types Of Smart Materials.....	3
1.4 Applications Of Smart Materials	4
1.5 Fundamentals Of Aerodynamics	4
1.5.1 The Four Forces.....	4
1.5.2 Coefficients Of Lift And Drag	5
1.5.3 Mach Number.....	5
CHAPTER 2 DESCRIPTION OF THE PROBLEM GEOMETRY	7
CHAPTER 3 DESIGNING BENDING AIRFOIL	9
3.1 Bending Beam Method.....	9
3.1.1. Bending Equation Formation.....	9
3.1.2. Airfoil with Bending Profile	12
3.1.3. Identification of Important Profiles.....	13
3.1.4. Determination of the Coordinate at which the Arc Length is Constant.....	14
3.1.5. Matlab Algorithm.....	15
3.1.6. Formulation of The Upper And Lower Curve Equations	16
3.1.7. Creation of Data Files	17
3.2 Tangent Arc Method.....	17
3.2.1. Introduction	17
3.2.2. Designing the Bending Profile.....	19
3.2.3. Data Collection	20
CHAPTER 4 MESHING AND DEFINING BOUNDARY CONDITIONS	21
4.1 Mesh Generation Using Gambit	21
4.2. Boundary Conditions	23

CHAPTER 5	NUMERICAL METHOD	24
5.1	Governing Equations For Flow Over Smart Wings	24
5.2	Fluid Dynamics Models.....	25
5.2.1	Spalart-Allmaras Model.....	25
5.3	The Coupled Solver	26
5.4	Linearization.....	26
5.4.1.	Implicit Method	27
5.4.2.	Explicit Method	27
CHAPTER 6	RESULTS AND DISCUSSION.....	28
6.1	NACA 1412 With Bending Beam Method.....	28
6.2	NACA 1412 With Circular Arc Method.....	33
6.3	Bench Marking Problem.....	39
6.4	Validation.....	48
6.5	Effect of Changing Pivot Point.....	49
CHAPTER 7	CONCLUSION AND SUGGESTIONS	54
REFERENCES	56
VITA	59

LIST OF FIGURES

Figure 2.1	Schematic Diagram of the Flow Field.....	7
Figure.3.1	Cantilever Beam with Uniformly Varying Load with Roller Support at the Free End.....	10
Figure 3.2	Determination of the Bending Profile Coefficients.....	11
Figure 3.3	Finite Bending Profiles.....	12
Figure 3.4	Bending Profile with NACA1412	13
Figure 3.5	Selected Important Profiles	14
Figure 3.6	Curves with Constant Arc Lengths.....	16
Figure 3.7	Completed Model of a Bending Airfoil.....	16
Figure 3.8	Tangent Arc Method (a) Intersecting Circles (b) Take off Flap Profile (c) Landing Flap Profile.....	19
Figure 3.9	NACA 1412 new design for take off position.....	20
Figure 4.1	Computational Domain Geometry	22
Figure 4.2	Meshed Model of a Parametric Smart Airfoil (Landing)	22
Figure 6.1	Meshed Model of a Parametric Conventional Airfoil At $\delta = -15^\circ$	29
Figure 6.2	Meshed Model of a Parametric Smart Airfoil At $\delta = -15^\circ$	29
Figure 6.3	Velocity (m/s) Contours at Landing Position for a Parametric Flexible airfoil.....	30
Figure 6.4	Velocity (m/s) Contours at Landing Position for a Parametric Conventional Airfoil.....	31
Figure 6.5	Pressure (Pa) Contours at $\delta = -15^\circ$ for a Parametric Flexible Airfoil.....	32
Figure 6.6	Pressure (Pa) Contours at $\delta = -15^\circ$ for a Parametric Conventional Airfoil ...	32
Figure 6.7	Pressure (Pa) Contours at $\alpha = 0, \delta = 5^\circ$ for a Parametric Conventional Airfoil.....	35
Figure 6.8	Pressure (Pa) Contours at $\alpha = 0, \delta = 5^\circ$ for a Parametric Smart Airfoil.....	35
Figure 6.9	Velocity (m/s) Contours at $\alpha = 0, \delta = 5^\circ$ for a Parametric Conventional Airfoil.....	36
Figure 6.10	Velocity (m/s) Contours at $\alpha = 0, \delta = 5^\circ$ for a Parametric Smart Airfo	36
Figure 6.11	Plot between Angle of Attack and Coefficients of Lift, Drag at $\delta = 15^\circ, Ma = 0.22$	39
Figure 6.12	Lift Characteristics of NACA 66215-216 Airfoil with Sealed Flap.....	40
Figure 6.13	Meshed Model of NACA 66215-216 Airfoil.....	41
Figure 6.14	Pressure (Pa) Contours ($\delta = 0^\circ, \alpha = 0^\circ$)	42
Figure 6.15	Meshed Model for $\delta = 5^\circ$	43
Figure 6.16	Pressure (Pa) Contours at $\alpha = 4^\circ, \delta = 5^\circ$	44
Figure 6.17	Pressure (Pa) Contours at $\alpha = 10^\circ, \delta = 5^\circ$	45
Figure 6.18	Meshed Model for $\delta = 15^\circ$	45
Figure 6.19	Pressure (Pa) Contours at $\alpha = 0^\circ, \delta = 15^\circ$	46
Figure 6.20	Pressure (Pa) Contours at $\alpha = 4^\circ, \delta = 15^\circ$	47

Figure 6.21	Pressure (Pa) Contours at $\alpha = 10^\circ, \delta = 15^\circ$	47
Figure 6.22	Pressure (Pa) Contours at $\alpha = 16^\circ, \delta = 15^\circ$	48

LIST OF TABLES

Table 6.1	Comparison of Lift and Drag Values at $Ma=0.8$, $\delta= 23^\circ$	30
Table 6.2	Comparison of Lift and Drag Values at $Ma=0.8$, $\delta= 50^\circ$	30
Table 6.3	Comparison of Lift and Drag Values at $Ma=0.8$, $\delta= -50^\circ$	33
Table 6.4	Comparison of Lift and Drag Values at $Ma=0.8$, $\delta= 5^\circ$	34
Table 6.5	Comparison of Lift and Drag Values at $Ma=0.8$, $\delta= 15^\circ$	37
Table 6.6	Comparison of Lift and Drag Values at $Ma=0.22$, $\delta= 5^\circ$	37
Table 6.7	Comparison of Lift and Drag Values at $Ma=0.8$, $\delta= 15^\circ$	38
Table 6.8	Comparison between $C_{L[1]}$ and $C_{Lsimulation}$ ($\delta=0^\circ$)	43
Table 6.9	Comparison between $C_{L[1]}$ and $C_{Lsimulation}$ ($\delta=5^\circ$)	44
Table 6.10	Comparison between $C_{L[1]}$ and $C_{Lsimulation}$ ($\delta=15^\circ$)	46
Table 6.11	Comparisons between Calculated and Experimental Aerodynamic Coefficients, Fully Turbulent Conditions	49
Table 6.12	Lift and Drag Characteristics at $0.85C$, $\delta=5^\circ$	50
Table 6.13	Lift and Drag Characteristics at $0.85C$, $\delta=15^\circ$	50
Table 6.14	Lift and Drag Characteristics at $0.85C$, $\delta= -10^\circ$	50
Table 6.15	Lift and Drag Characteristics at $0.75C$, $\delta=5^\circ$	51
Table 6.16	Lift and Drag Characteristics at $0.75C$, $\delta=15^\circ$	51
Table 6.17	Lift and Drag Characteristics at $0.75C$, $\delta=-10^\circ$	51
Table 6.18	Lift and Drag Characteristics at $0.80C$, $\delta=5^\circ$	52
Table 6.19	Lift and Drag Characteristics at $0.80C$, $\delta=15^\circ$	52
Table 6.20	Lift and Drag Characteristics at $0.80C$, $\delta= -10^\circ$	52

ACKNOWLEDGMENTS

I dedicate this work to my parents who have always wished life's best things for me. I like to express my heartfelt gratitude to my advisor Dr. Yitung Chen for funding this project. I appreciate his keen interest in the well being of his students and I thank him for guiding and constantly motivating me throughout the course work. He was always there when I needed direction and I had a very nice time working with him.

Thanks are due to Dr. Sahjendra Singh, Dr. Woosoon Yim and Dr. William Culbreth, for being part of my thesis committee.

I thank my elder brother Muruganandhan—who always offers valuable advice, and all my family members for their emotional support. I would like to make a special mention about my well wisher “Cavalier” M.S. Mathivanan, for his support and positive thoughts. I would also like to thank my best friends Ravishankar, Ashwini and their family, for their words of comfort and guidance.

I would like to take this opportunity to thank John Ligon family for their love and affection and my high school teachers Mr. Natarajan, Mr. Gopalan, Mr. Saravanan and Mr. Shanmuga Sundaram, whose good wishes are a constant source of energy.

NOMENCLATURE

C_d	coefficient of drag
C_l	coefficient of lift
L	lift force (N/m^2)
D	drag force (N/m^2)
q_∞	dynamic pressure (N/m^2)
S	reference area (m^2)
M	Mach number
E	Young's modulus
I	area moment of inertia (m^4)
L	length of the beam (m)
Y	equation of upper/lower curve
N	number of differences
Y_e	y-coordinate of the curve at constant arc length
X_e	x-coordinate of the curve at constant arc length
a	speed of sound (m/s)
e	internal energy (J)
F	force (N)
k	turbulent kinetic energy (J)
P	total pressure (N/m^2)
p	static pressure (N/m^2)
Re	Reynolds number
t	time (s)
T	static temperature ($^{\circ}C$)
u	x-component of velocity (m/s)
v	y-component of velocity (m/s)
w	z-component of velocity (m/s)
x	horizontal Cartesian coordinate
y	vertical Cartesian coordinate

Greek Symbols

α	angle of attack ($^{\circ}C$)
z	lateral Cartesian coordinate
μ	dynamic viscosity ($N.s/m^2$)
μ_T	turbulent dynamic viscosity ($N.s/m^2$)
τ	viscous stress tensor
ν	kinematic viscosity (m^2/s)
ρ	density (Kg/m^3)

Subscripts

Lconv	lift, conventional airfoil
Lsmart	lift, smart airfoil
Dconv	drag, conventional airfoil
Dsmart	drag, smart airfoil
L[1]	lift, paper
Lsimulation	lift, simulation

CHAPTER 1

INTRODUCTION

Airplanes—Modern world badly needs this creation of Wright brothers. There has been lot of changes in the design and operation of the aircraft, since their invention. And they are getting better and better with the idea and vision of the scientists all over the world. At the advent of smart materials, adaptive wings—the wings which can change its shape and size—is going to be a reality. These bending wings seem to have many advantages over conventional airfoils. Since the smart wings are in their developing stage study of fluid dynamics around them will be of very much importance once the design is complete. This attempt is an initiative in the path of identifying the best bending profiles that the wings can morph during take off, cruise and landing. In this study a parametric design is created for the adaptive wing and its performance characteristics are analyzed. The focus has been on two-dimensional design of a smart airfoil and Computational Fluid Dynamics (CFD) modeling of them. This model can further be expanded to three-dimensional bending airfoils and flapping flights.

1.1 History of Wings

George Cayley (1773-1857) was the father of aerodynamics. His 1804 glider model incorporated most design elements of a modern airplane. Alphonse Penaud (1850-80) built a rubber band powered "piano-phore" model; its 131-foot flight was the first of an inherently stable aircraft. Otto Lilienthal (1848-96) was the first true glider pilot. Inspired, the Wrights took up his quest to get on "intimate terms with the wind". Octave Chanute (1832-1910) gathered and disseminated aeronautical knowledge. He encouraged the Wrights, who used his biplane glider design. The dream project of Wilbur and Orville Wright didn't emerge without failures. The design of their glider needed major changes to be a success. These explorers didn't agree with the existing scientific data and went on to find their own [4]. They built a square wind tunnel powered by a two bladed fan connected to a gasoline engine. They tested almost all the shapes an airfoil could possibly take. Curved plates, rounded leading edges, rectangular and curved platforms, and various monoplane and multiplane configurations were among those designs. The aerodynamic data was taken logically and carefully. They succeeded flying their glider with this new airfoil design data. Since then, there has been lots of advancement in the design of airfoils. Smart airfoils—a shape changing wing is the task of current generation aerodynamists. This study is aimed at obtaining airfoil data for a parametric smart airfoil, which might be used in future applications.

1.2 Smart Wings

A smart wing is one which uses smart materials for the shape control of its surface. This model would improve aircraft efficiency and performance, since it doesn't have hinges and is aerodynamically perfect. Smart materials have unique properties. These wings use non-hydraulic based actuators which can be piezoelectric devices or shape memory alloys [2]. Hydraulic actuators are heavy and on the contrary smart wings are way too light. Since this study deals with the investigation of shape effects, smart material property functions are not considered here.

1.3 Types of Smart Materials

There are different types of smart materials available. Some of them are discussed here. Piezoelectric or electrostrictive material will deform when subjected to an electric charge or a variation in voltage. Electrostrictive materials produce displacements in same direction where as Piezoelectric materials can deform in both the direction under compression and elongation [2]. Magnetostrictive materials undergo induced mechanical strain when subjected to a magnetic field. Terfenol-D [3] is a very good example for these kinds of materials. Shape Memory Alloys will undergo phase transformations which will produce shape changes when subjected to a thermal field. With low temperature, it deforms to its 'martensitic' condition and regains its original shape in its 'austenite' condition when heated. Nitinol TiNi [3] is an example of shape memory alloys.

1.4 Applications of Smart Materials

Piezoelectric materials are most widely used as sensors in different environments. They are often used to measure fluid compositions, fluid density, fluid viscosity, or the force of an impact. Shape memory alloys are used in several applications, like in surgical tools and muscle wires. One important application of them in the field of aeronautics is flexible wings. Shape memory alloys exhibit two unique properties, pseudo elasticity—which is a rubber like behavior of material, and the shape memory effect. Our major focus falls on those materials used for the construction of flaps. Alternatives to the hydraulic systems are being explored by the aerospace industry. Among the most promising alternatives are piezoelectric fibers, electrostrictive ceramics, and shape memory alloys.

1.5 Fundamentals of Aerodynamics

1.5.1 The Four Forces

Lift, drag, thrust, weight are known as the four forces. The component of aerodynamic force perpendicular to the relative wind is known as lift force. The downward force due to the weight of the aircraft is called weight force. Lift force has to be more than the weight in order to achieve flying. The forward force produced by the engine is thrust force. It acts along the axis of the engine. The aerodynamic force parallel to the relative wind is called drag force. Thrust force should be more than the drag force in order to cause a forward motion of the air plane.

1.5.2 Coefficients of Lift and Drag

Lift coefficient [4] is given by the equation,

$$C_L = \frac{L}{q_\infty \times S} \quad (1.1)$$

and drag coefficient is give by,

$$C_D = \frac{D}{q_\infty \times S} \quad (1.2)$$

where,

L is the lift force (N),

D is the drag force (N),

q_∞ is the dynamic pressure (N/m²),

and S is the reference area (m²)

The pressure of a fluid resulting from its motion is defined as dynamic pressure. It is given by the following equation [4],

$$q_\infty = \frac{1}{2} \rho_\infty V_\infty^2 \quad (1.3)$$

ρ_∞ and V_∞ are density and velocity respectively in the free stream far ahead of the body.

1.5.3 Mach Number

The ratio between the velocity of the fluid and the velocity of the sound is known as Mach number. Airplanes have different speeds at different instances. Though the speed is

described in knots conventionally, researchers in the field of fluid dynamics prefer to use it in terms of Mach number and/or Reynolds number.

CHAPTER 2

DESCRIPTION OF THE PROBLEM GEOMETRY

Two different models are considered here for the design of smart airfoils. First method used for the determination of the bending profile of the airfoil is bending beam method. And, the second one is tangent arc method. In both the cases the computational fluid dynamics model is similar, except that it has a little variation in the profile of the bending flap. For the former model, the Mach number is taken as 0.8 and for the later case, two different speeds ($Ma=0.80$ and 0.22) are used. The model is shown in Figure 2.1 below.

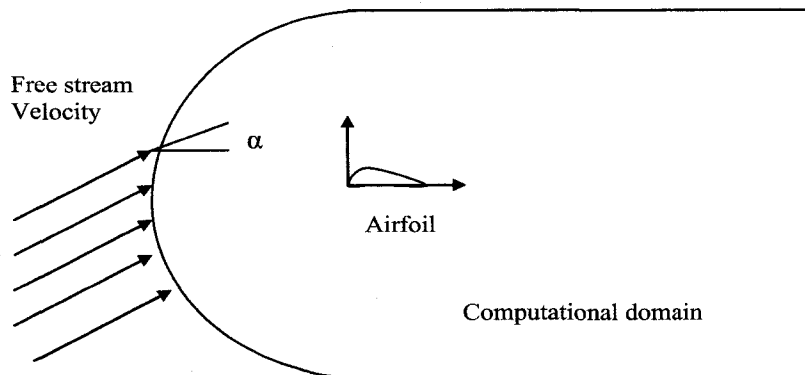


Figure 2.1 Schematic diagram of the flow field

It should be noted that in each design method there are different take off and landing positions considered. 5° and 15° flap deflection angles are considered (for take off), since they are the most commonly used take off positions [5]. Usually for landing 40° flap deflection angle is considered. Since the study doesn't include slats in the analysis, actual conventional landing conditions are not considered here. Instead a parametric conventional model is considered. The details of the model are discussed in the following chapters.

The velocity of the fluid far away from the control volume is generally known as free stream velocity. α is known to be the angle of attack—the angle between the moving object and the relative wind. One of the major tasks of this project is to analyze the effect of lift and drag values for different angles of attack and for different flap deflection angles. Flap deflection angle is defined as the angle between the chord line of an airfoil and the deflected flap. Usually, flights take off in the range of 260 km/hr – 290 km/hr [5]. The Mach number is calculated as shown below.

$$\text{Mach number} = \frac{\text{Speed of the object (m/s)}}{\text{Speed of sound (m/s) at standard sea level temperature}} \quad (2.1)$$

Hence,

$$\text{Ma} = 72.22 / 340$$

This gives, $\text{Ma} = 0.212$

But in our study the first speed is taken as $\text{Ma}=0.22$. Similarly for the second range of speed 290 km/hr the Mach number $\text{Ma}= 0.24$ can be obtained. These two speeds are used in the CFD simulations for the parametric conventional and smart airfoils and the effects were analyzed.

CHAPTER 3

DESIGNING BENDING AIRFOIL

The flexible airfoil was designed in two different ways during this study. Only the possible shape changes in trailing edge are considered. Details regarding the use of smart materials in the leading edge can be found in reference [2]. Following are the two methods used to design the smart flaps.

- i) Bending beam method
- ii) Tangent arc method

3.1 Bending Beam Method

3.1.1 Bending Equation Formation

NACA 1412 airfoil is chosen for the analysis. A parametric bending profile is formulated as stated below. Different types of beams were analyzed [22] to find the bending equation of an adaptive wing. Equations of fixed beam with pointed load, fixed beams with uniformly varying load, fixed beams with uniform load, cantilever beam with point load on the free end, cantilever beam with roller support in the free end, cantilever beam with uniformly varying load with roller support in the free end, were considered. The bending profile of the cantilever beam with uniformly varying load with roller support at the free end (Figure 3.1) may resemble the bending profile of an adaptive wing. The profile of the beam is given below.

$$y = \frac{w_0(-x^5 + 2L^2x^3 - L^4x)}{120EIL} \quad (3.1)$$

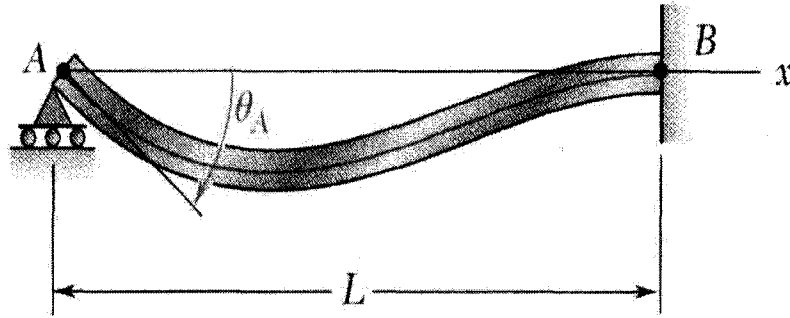


Figure 3.1 Cantilever beam with uniformly varying load with roller support at the free end

where,

w_0 = Weight/unit length (N/m)

E = Young's modulus

I = Area moment of inertia (m⁴)

L = length of the beam (m)

The above bending equation can be taken to manipulate the coordinates of the bending airfoil by making minor modifications. Since the parametric equation alone is desired, which would give a similar profile, all the other loads and constant values given in the above equation are neglected.

The modified equations are found to be,

$$Y_{\text{landing}} = (-x^5 - 1.2x^3 + x)/2 \quad (3.2)$$

$$Y_{\text{takeoff}} = (-x^5 - 1.2x^3 + x)/2 \quad (3.3)$$

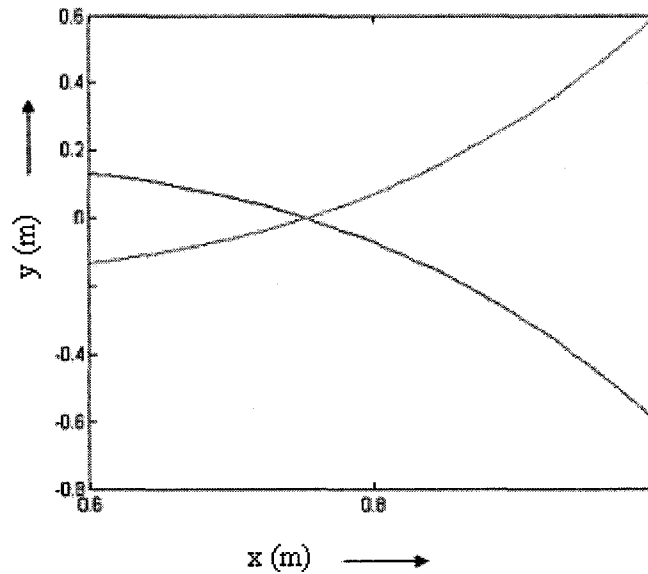


Figure 3.2 Determination of the bending profile coefficients

The coefficients of equations (3.2) & (3.3) are determined by iterative process. Each profile is visualized using MATLAB, and the value of the coefficient is either increased or decreased until the desired profile is obtained. These equations are used only to begin the investigation and could be modified to obtain the optimum design in the future. The point at which these two curves intersect is to be found, to locate the pivot point. When the equation is solved, the x coordinate can be found to be $x=0.75$. The next step of the problem is to find the coefficients of the equation for different bending positions. The

coefficients are found to be 0.5, 0.4, 0.333, 0.2857, 0.25, 0.1666, 0.125, 0.0909, 0.0625, and 0.04. The MATLAB plots of the finite bending curve using the above coefficients are shown in Figure.3.3.

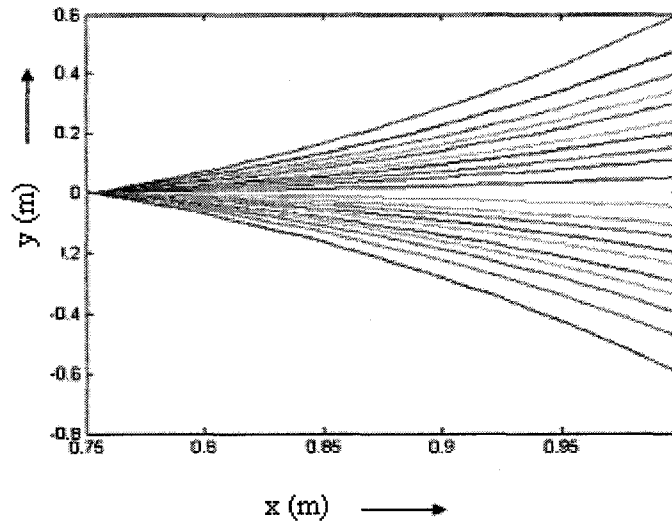


Figure 3.3 Finite bending profiles

3.1.2 Airfoil with Bending Profile

With the equations and coefficients in hand the finite bending profile is found. This profile is merged with the NACA 1412 (see Figure 3.4) to see if that gives a reasonable bending shape. After this, it can be seen that there are several other problems to be sorted out. Choosing important curves (or positions) that would contribute to this study, setting constant arc length for all the curves, are some among them. It has been discussed elaborately in the following sections.

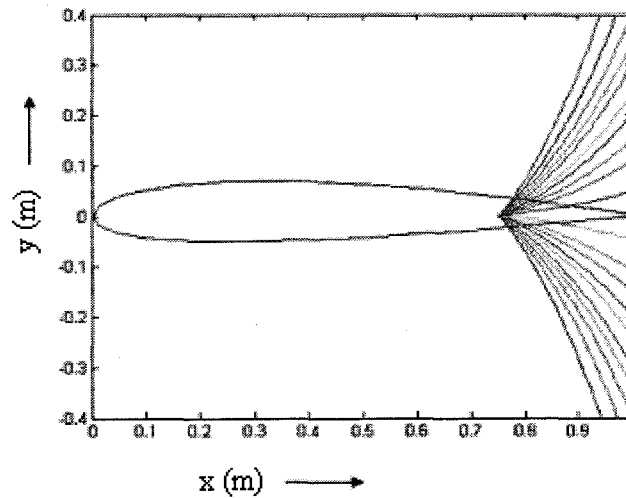


Figure 3.4 Bending profile with NACA1412

3.1.3 Identification of Important Profiles

Now that there are several equations to analyze the finite bending of airfoil, it is essential to choose the crucial ones. The curves shown in Figure 3.5 are chosen for the analysis. It can be seen that the curves have different arc lengths. But, it is necessary that the curves have constant arc length. The coordinates of the point on each curve where the arc length is constant are determined in the following section.

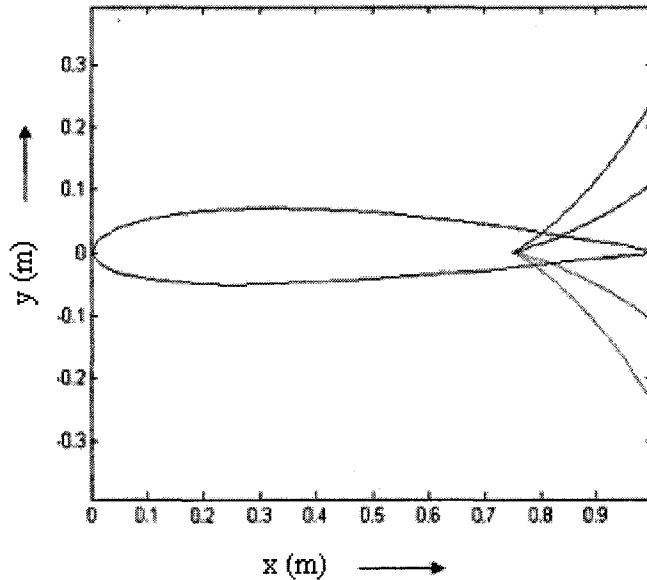


Figure 3.5 Selected important profiles

3.1.4. Determination of the Coordinate at which the Arc Length is Constant

Since the bending equation obtained is a 5th order polynomial equation, coordinate at which the arc length is constant is determined by numerical method. The arc length is known to be the distance between pivot point and the end point (at $y=0$) of the airfoil, which is $=0.25$. This value needs to be constant for all the curves. The point at which this length is equal to the arc length is found using Pythagorean Theorem. The y coordinates at $x = 1$ is divided into 26 equal parts. Therefore, $dy = Y_e / 26$, and since we know the arc length $= 0.25$, $dx = 0.001$. By Pythagorean Theorem, $N =$ no of division where arc length becomes equal to 0.25. Once the N value is determined the unknowns can be easily calculated. The N value is obtained from a MATLAB program.

3.1.5 MATLAB Algorithm

A MATLAB program is written to find the coordinates where the arc length is constant. N is the number of differences needed so that when multiplied by dy we get the constant arc length for a particular curve. N value is found using equation (3.4) and (3.5). The coordinates of the point (X_e, Y_e) at constant arc length is then determined.

$$N \times \sqrt{dx^2 + dy^2} = 0.25 \quad (3.4)$$

Hence,

$$N = 0.25 / \sqrt{dx^2 + dy^2} \quad (3.5)$$

$$Y_e = dy \times N \quad (3.5.a)$$

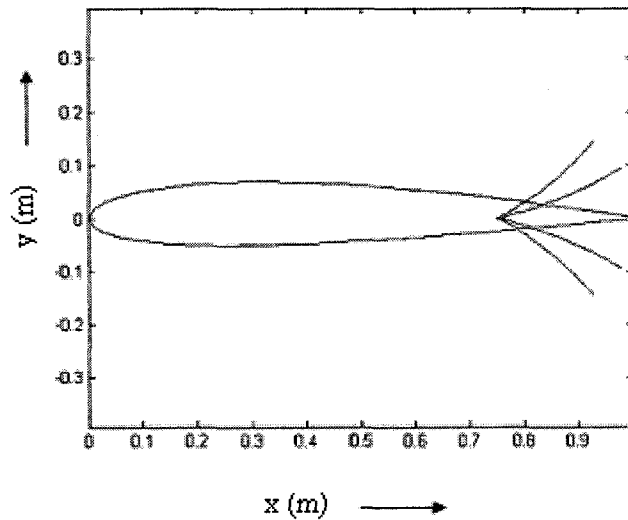


Figure 3.6 Curves with constant arc length

$$X_e = 0.75 + dy \times N \quad (3.5.b)$$

The results are displayed in fig. 3.6 for all the four curves

3.1.6. Formulation of the Upper and Lower Curve Equations

The next task would be to find the equation for the upper and lower curves. We know the family of equations with point P (0.75, 0) as origin. From interpolation the upper and lower coordinates are found to be $y=0.038$, $y=-0.024$. These values are obtained from the equations of NACA four digit airfoil.

The upper curve equation would be

$$Y=0.038+ (\text{equation (3.2)} \times \text{coefficient}) \quad (3.6)$$

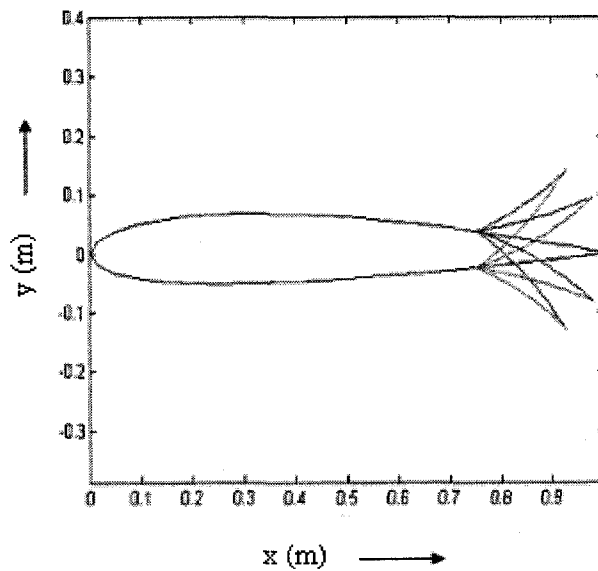


Figure 3.7 Completed model of a bending airfoil

The lower curve equation would be,

$$Y = -0.024 + (\text{equation (3.2)} \times \text{coefficient}) \quad (3.7)$$

Equation (3.3) can be used in place of equation (3.2) in equations (3.6) and (3.7), while it is necessary to formulate the downward bending curves. The coefficients can be calculated using the results of the constant arc length MATLAB program. Similarly, the coefficients are obtained for all the four curves. Finally the coordinates of the bending curve are plotted using MATLAB. From Figure 3.7, the different positions of the bending airfoil can be seen.

3.1.7 Creation of Data Files

A data file for each bending position has to be created. Since the design involves six different equations, the coordinates are arranged in anti-clockwise direction. This is done by using Microsoft Excel worksheets. Finally the data files are created and saved in separate folders for future use.

3.2 Tangent Arc Method

3.2.1 Introduction

Bending beam method [17] is not the only way one could design the bending profile of a smart airfoil. Bending profiles might also involve complex equations. Tangent arc method of designing bending airfoils is described below. An arc drawn tangent to the upper, lower surface of the airfoil at the pivot point to the end point of the airfoil gives a smooth profile. Figure 3.8 shows SOLID WORKS sketch of tangent arc method. There are two arcs involved in any one position. For different flap deflection angle, the tangent arc has different radius and also the center of the arc keeps changing.

Accurate methods can be devised to track those points in future study. Current study limits itself to the design and analysis of the smart wing using tangent arc method.

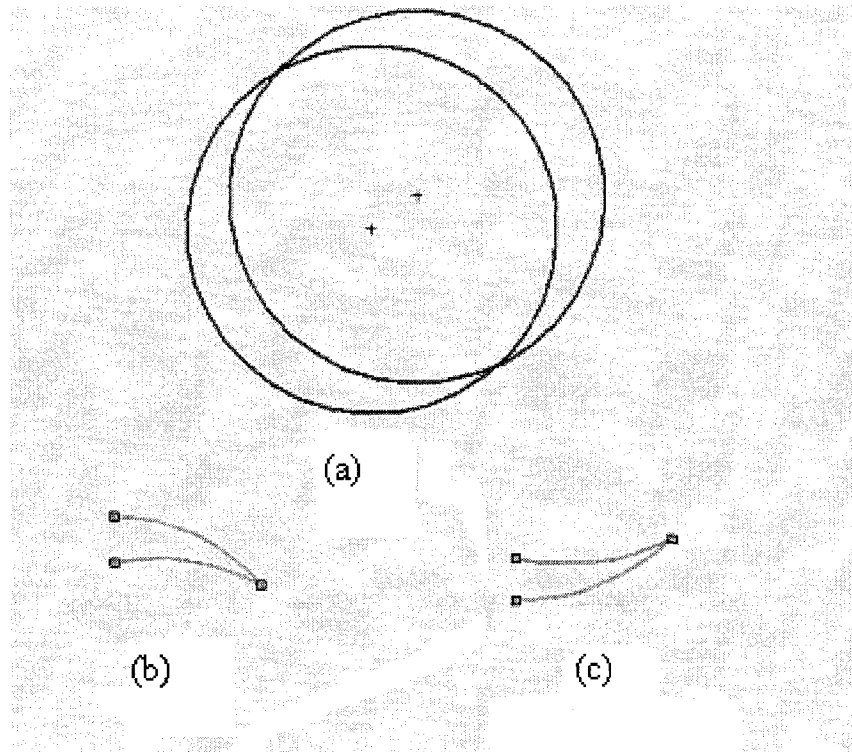


Figure 3.8 Tangent arc method. (a) Intersecting circles, (b) Take off flap profile, (c) Landing Flap Profile

3.2.2 Designing the Bending Profile

The airfoil coordinates are plotted in the SOLIDWORKS work space. NACA 1412 and BAC XXX airfoils are selected for the analysis. The pivot point is selected as 0.8m from the leading edge initially. Later on—during the investigation on the effect of changing pivot point, different pivot points are used. The design is created for the selected four positions of the airfoil. Two positions during landing and two positions during take off. The end points are known for different flap deflection angle and hence the end points are plotted. Using the options available in the SOLIDWORKS user interface, tangent arcs are drawn for both the upper and bottom part of the flap (see figure 3.9).

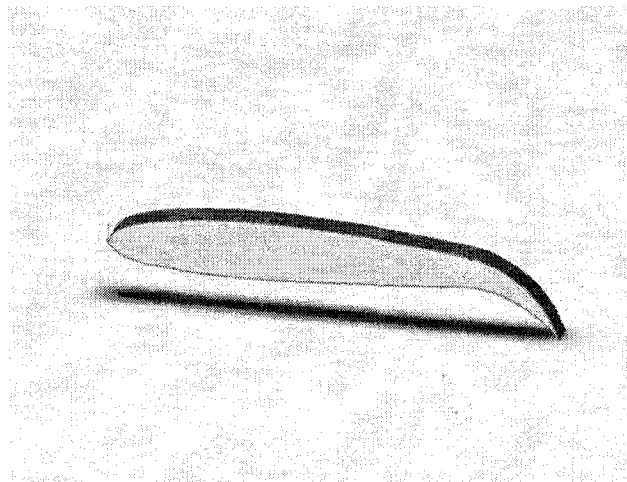


Figure 3.9 NACA 1412 new design for take off position

3.2.3 Data Collection

The data relevant to each design is noted down and stored in a separate file. Later on these data files can be imported to create mesh files in GAMBIT. Important data includes the arc radius for each curve and the positions of them relative to the x and y axis. The set of data file is completed. Now the mesh files of the model can be created and the fluid dynamics around the smart airfoil can be analyzed.

CHAPTER 4

MESHING AND DEFINING BOUNDARY CONDITIONS

With all the data extracted from MATLAB code and SOLID WORKS modeling, data files are created. This topic addresses how the meshing is done and boundary conditions are assigned using GAMBIT.

4.1 Mesh Generation Using Gambit

Data files created in the previous section are imported to the GAMBIT-working directory. The vertex data are read using the command “import vertex data filename. txt”. The two-dimensional airfoil is created using Non-Uniform Rational B-Spline (NURBS) command. The dimensions of the computational domain are shown in Figure 4.1. The computational domain is created using straight lines and arcs with afore mentioned dimensions. In Bending Beam Method, the data file contains coordinates of the entire airfoil i.e., including flaps. But in Tangent Arc Method the data file has coordinates till the pivot point. The radius and center points of the upper and lower arc of the bending flaps are noted down from the SOLIDWORKS model. Those values are used here in GAMBIT to design the flap. Node points are created on each edge of the computational domain and the airfoil using “Mesh Edge” command button. Faces are generated from the available edges.

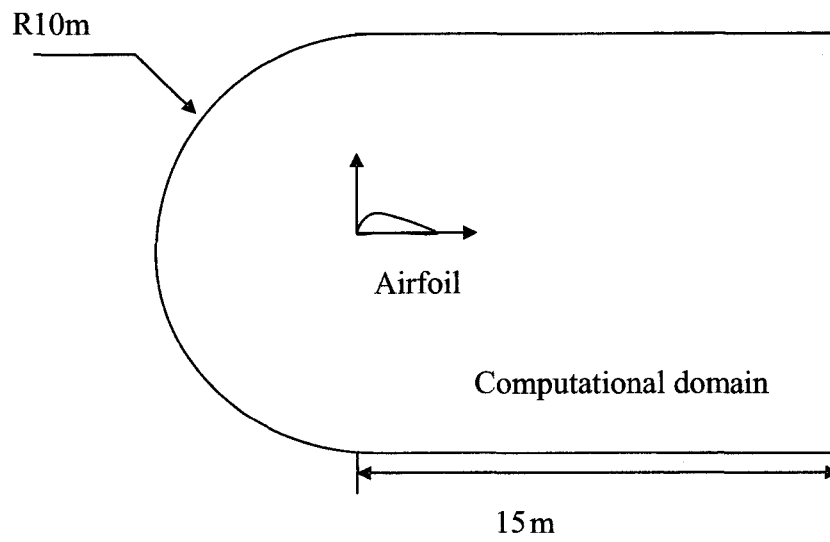


Figure 4.1 Computational domain geometry

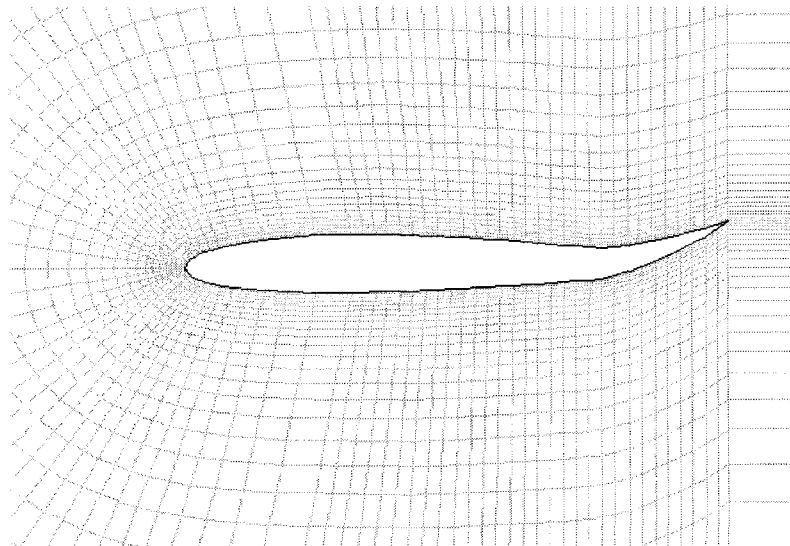


Figure 4.2 Meshed model of a parametric smart airfoil (landing)

Then using “Mesh Faces” command button the faces are meshed. Map method is selected for meshing. Finally the mesh is generated. The mesh file is shown in Figure 4.2.

4.2. Boundary Conditions

In order for the mesh to be properly transferred to FLUENT, the edges must be assigned boundary conditions, such as wall, inlet, outlet, etc. Actual numerical values will be specified from within FLUENT itself. In operations field, “zones command button-specific boundary types command button”, can be found. The airfoil is assigned “wall” type boundary condition. The flow field far away from the airfoil is assigned “pressure far field” boundary condition. “Interior” boundary condition is assigned to the interior edges that were used to construct the far-field. Now the file is saved and written out in the format used by FLUENT.

CHAPTER 5

NUMERICAL METHOD

The flow over a two-dimensional airfoil is solved using numerical method. This section deals with the numerical method adopted for the study of our problem. The Spalart-Allmaras turbulence model is used here. Coupled solver is selected and linearization is done using implicit method.

5.1 Governing Equations for Flow over Smart Wings

There are two common methods for formulating the fluid dynamics model of an airfoil. The method, which uses Navier-Stokes equation and a method called Doublet lattice method. The Navier-Stokes equation can be used for the flexible wing problem [2]. The governing equation of fluid dynamics in 2-D Cartesian coordinates can be represented as

$$\frac{\partial Q}{\partial t} + \frac{\partial F}{\partial x} + \frac{\partial G}{\partial y} = \frac{\partial J_x}{\partial x} + \frac{\partial J_y}{\partial y} \quad (5.1)$$

$$\text{where } Q = \begin{pmatrix} \rho \\ \rho u \\ \rho v \\ \rho e \end{pmatrix}, F = \begin{pmatrix} \rho u \\ \rho u^2 + p \\ \rho u \\ \rho e u + p u \end{pmatrix}, G = \begin{pmatrix} \rho v \\ \rho u v \\ \rho v^2 + p \\ \rho e v + p v \end{pmatrix}$$

$$J_x = \begin{pmatrix} 0 \\ \tau_{xy} \\ \tau_{yy} \\ k_x \frac{\partial T}{\partial x} + u\tau_{xx} + v\tau_{xy} \end{pmatrix}, J_y = \begin{pmatrix} 0 \\ \tau_{xx} \\ \tau_{xy} \\ k_y \frac{\partial T}{\partial y} + u\tau_{xy} + v\tau_{yy} \end{pmatrix}$$

Since there is no analytical solution to the equation 5.1 It can be solved using finite differences or finite volume method. In finite volume method the equation is converted into integral equation by using Gauss Divergence theorem. FLUENT uses finite volume method to solve fluid dynamics problems.

5.2 Fluid Dynamics Models

Turbulence modeling has been a challenging problem for scientists. Accurate turbulence models are very difficult to formulate [2]. Examples of simpler turbulence models include K-ε model and Spalart-Allmaras model. The later is used in our study. Reynolds five-equation model is an example for advanced turbulence models.

5.2.1 Spalart-Allmaras Model

The Spalart-Allmaras model was designed specifically for aerospace applications involving wall-bounded flows and has been shown to give good results for boundary layers subjected to adverse pressure gradients. The Spalart-Allmaras model is a relatively simple one-equation model that solves a modeled transport equation for the kinematic eddy (turbulent) viscosity. This embodies a relatively new class of one-equation models in which it is not necessary to calculate a length scale related to the local shear layer thickness.

5.3 The Coupled Solver

Two different solvers are available in FLUENT—the segregated solver and the coupled solver. The coupled solver solves the governing equations of continuity, momentum, and energy and species transport simultaneously. Governing equations for additional scalars will be solved sequentially (i.e., segregated from one another and from the coupled set). Because the governing equations are non-linear (and coupled), several iterations of the solution loop must be performed before a converged solution is obtained. Each iteration consists of the steps outlined below:

1. Fluid properties are updated, based on the current solution. (If the calculation has just begun, the properties will be updated based on the initialized solution.)
2. The continuity, momentum, and (where appropriate) energy and species equations are solved simultaneously.
3. Where appropriate, equations for scalars such as turbulence and radiation are solved using the previously updated values of the other variables.
4. When inter-phase coupling is to be included, the source terms in the appropriate continuous phase equations may be updated with a discrete phase trajectory calculation.
5. A check for convergence of the equation set is made.

These steps are continued until the convergence criteria are met.

5.4 Linearization

In both the segregated and coupled solution methods the discrete, non-linear governing equations are linearized to produce a system of equations for the dependent

variables in every computational cell. The resultant linear system is then solved to yield an updated flow-field solution. The manner in which the governing equations are linearized may take an "implicit" or "explicit" form with respect to the dependent variable (or set of variables) of interest.

5.4.1. Implicit Method

For a given variable, the unknown value in each cell is computed using a relation that includes both existing and unknown values from neighboring cells. Therefore each unknown will appear in more than one equation in the system, and these equations must be solved simultaneously to give the unknown quantities.

5.4.2. Explicit Method

For a given variable, the unknown value in each cell is computed using a relation that includes only the existing values. Therefore each unknown will appear in only one equation in the system and the equations for the unknown value in each cell can be solved one at a time to give the unknown quantities.

CHAPTER 6

RESULTS AND DISCUSSION

In this section the results are tabulated for all the cases investigated in the project. The primary focus was projected on finding lift and drag characteristics of parametric smart wing design and parametric conventional airfoil. Flow conditions around the airfoil are specified with the various options available from the FLUENT user interface. Coupled implicit method is used to determine the unknown velocity, pressure, and temperature profiles. Spalart-Allamaras turbulence model is used to solve the problem. Plots of pressure and velocity are shown for selected cases.

6.1 NACA 1412 with Bending Beam Method

The meshed files are imported to FLUENT user interface. The mesh files are checked for flaws. Then using the “display” menu option the grid is displayed. This step is essential one, since one can identify the undefined entities in the mesh file. The boundary conditions are defined. A Mach number of 0.8 was used for the analysis.

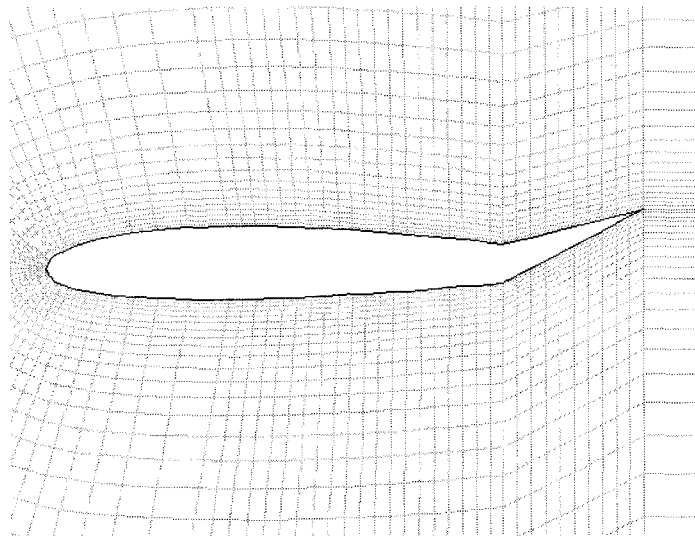


Figure 6.1 Meshed model of a parametric conventional airfoil at $\delta = -15^\circ$

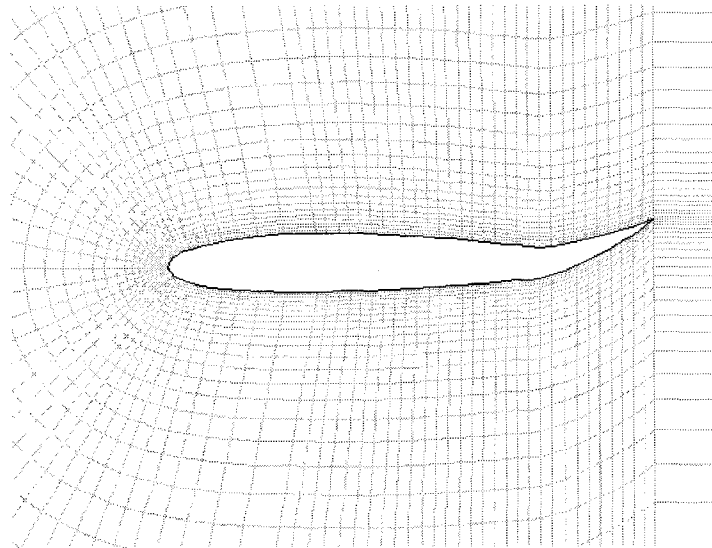


Figure 6.2 Meshed model of a parametric smart airfoil at $\delta = -15^\circ$

The lift and drag monitors are turned on. Co-efficient of lift and drag values are tabulated and the results were analyzed.

Table 6.1 Comparison of lift and drag values at $Ma=0.8$, $\delta=23^\circ$

	Conventional takeoff 1	Smart take off 1	% Increase
Coefficient of lift	1.27	1.36	7.08
Coefficient of Drag	0.1987	0.2200	10.71

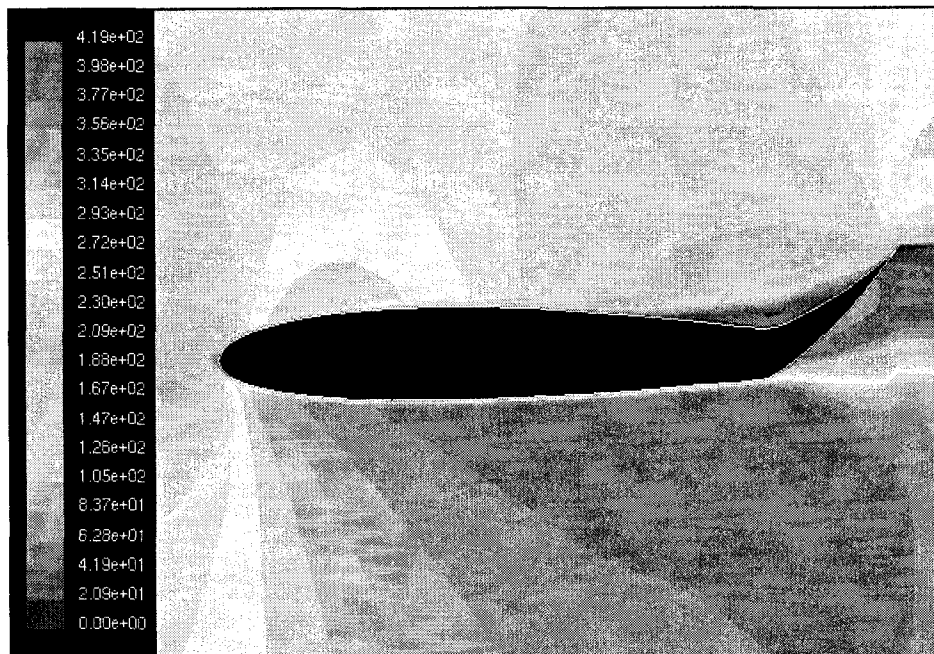


Figure 6.3 Velocity (m/s) contours at landing position for a parametric flexible airfoil

The results are displayed for 23 degree angle of attack and 0.8 Mach number. Lift and drag monitors are turned on to find the C_d and C_l . The velocity contours are shown in Figures 6.3, 6.4 and pressure contours are shown in Figures 6.5, 6.6

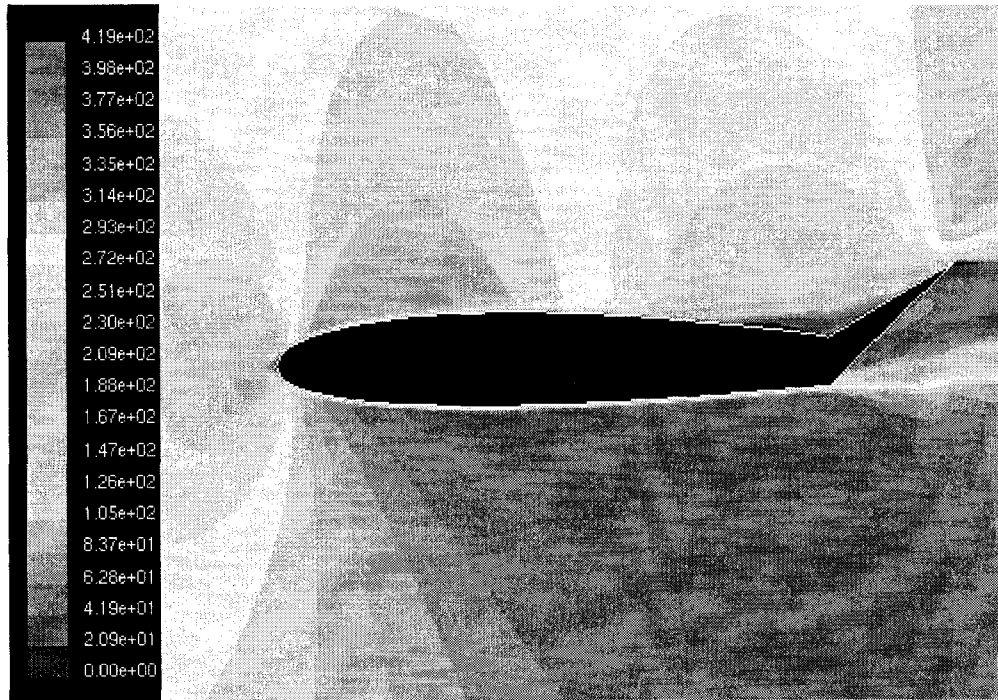


Figure 6.4 Velocity (m/s) contours at landing position for a parametric conventional airfoil

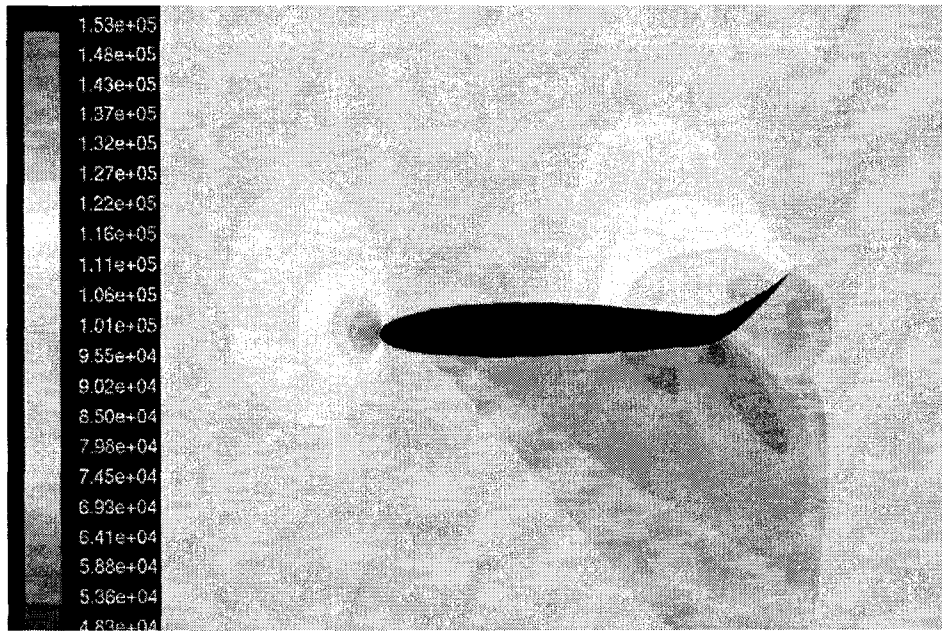


Figure 6.5 Pressure(Pa) contours at $\delta=-15^\circ$ for a parametric flexible airfoil

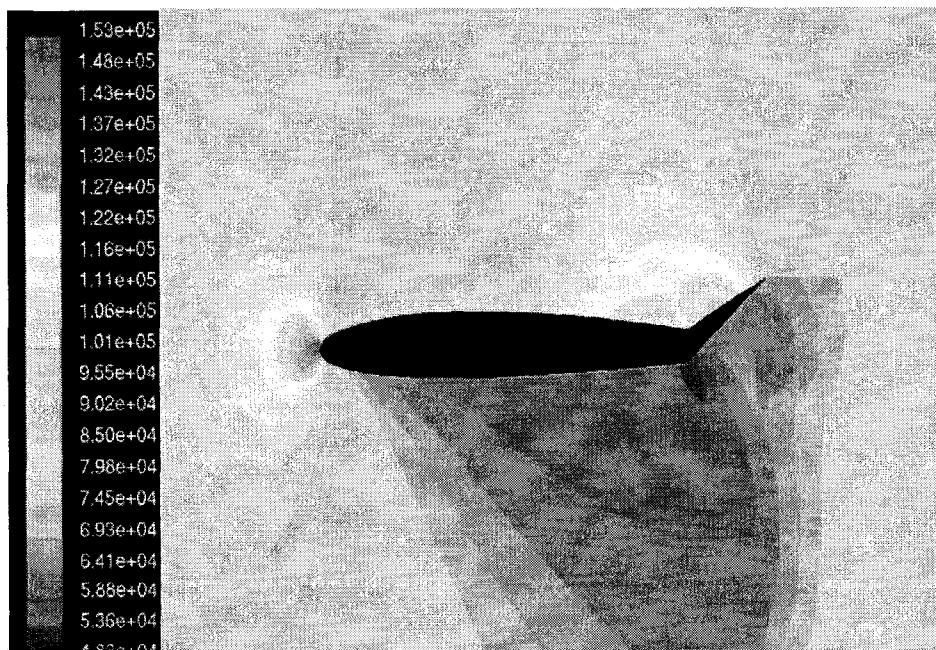


Figure 6.6 Pressure(Pa) contours at $\delta=-15^\circ$ for a parametric conventional airfoil

Table 6.2 Comparison of lift and drag values at $Ma=0.8, \delta= 50^\circ$

	Conventional airfoil	Smart airfoil	% Increase
Coefficient of lift	1.455	1.5037	3.35
Coefficient of Drag	0.285	0.2991	4.49

Table 6.3 Comparison of lift and drag values at $Ma=0.8, \delta= -50^\circ$

	Conventional landing 1	Smart landing 1	% Increase
Coefficient of lift	-0.7565	-0.8924	17.96
Coefficient of Drag	0.1131	0.1371	21.22

The lift and drag data obtained from the monitors give a reasonable improvement in negative lift and increase in drag which is good for landing. The parametric smart airfoil gives 17 % more negative lift and 21% more drag than that of the parametric conventional one. But for take off conditions the lift increased and the same time drag was also increased. The reason might be because of the fact that the bending beam design had some bumps in the flap which was formed by the bending profile. Early separation of the flow and the circulation causes increase in drag value. Hence the design was modified. The circular arc method is adopted after this analysis. The results are analyzed in the next section.

6.2 NACA 1412 with Circular Arc Method

Similar to the previous case the mesh files are imported to FLUENT. The same boundary conditions were applied . The coefficient of lift and drag values were tabulated as follows. Since good results for the smart landing positions in the previous case have been found, our objective here after would be to analyze the take off conditions of a smart wing. Table 6.4 and Table 6.5 show the values of increase in lift and drag values for take off position 1 and take off position 2, respectively. Take off position 1 has 5 degrees of flap deflection and take off position 2 has 15 degrees.

Table 6.4 Comparison of Lift and Drag Values at $Ma=0.8$, $\delta= 5^\circ$

α (deg)	C_{Lconv}	C_{Lsmart}	%increase	C_{Dconv}	C_{Dsmart}	%increase
0°	0.88	1.05	19	0.098	0.121	22
5°	1.25	1.41	12.8	0.202	.2350	16.36
10°	1.42	1.52	7	0.32	0.348	8.75
15°	1.34	1.4	4.48	0.41	0.44	3

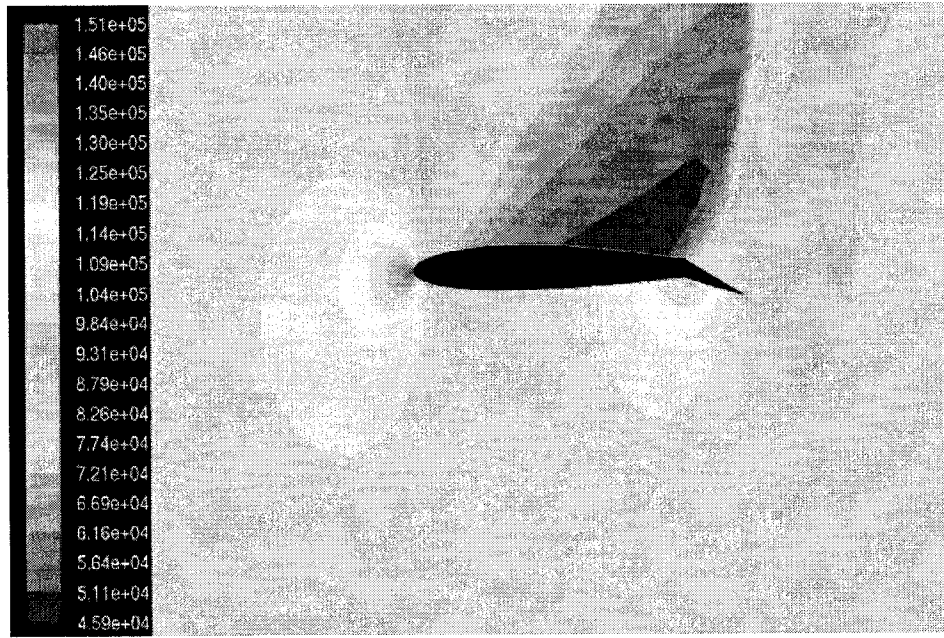


Figure 6.7 Pressure (Pa) contours at $\alpha=0$, $\delta=5^\circ$ for a parametric conventional airfoil

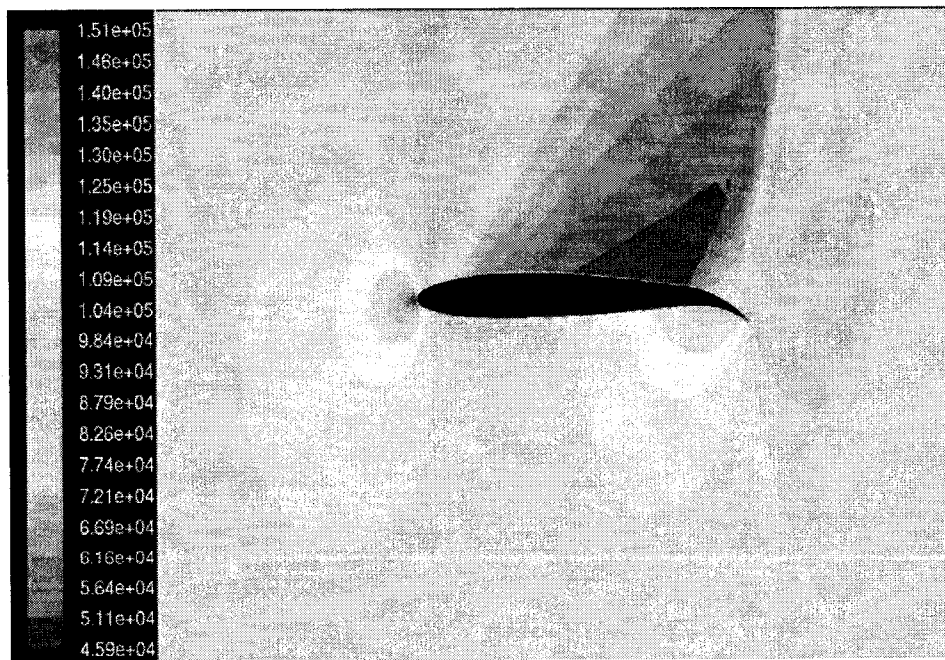


Figure 6.8 Pressure (Pa) contours at $\alpha=0$, $\delta=5^\circ$ for a parametric smart airfoil

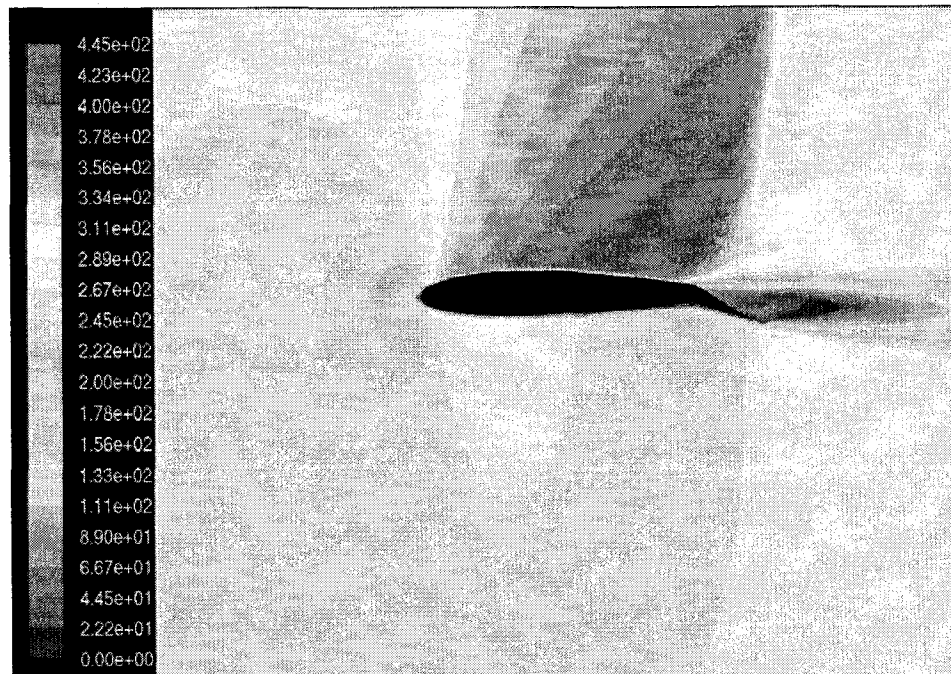


Figure 6.9 Velocity (m/s) contours at $\alpha=0$, $\delta=5^\circ$ for a parametric conventional airfoil

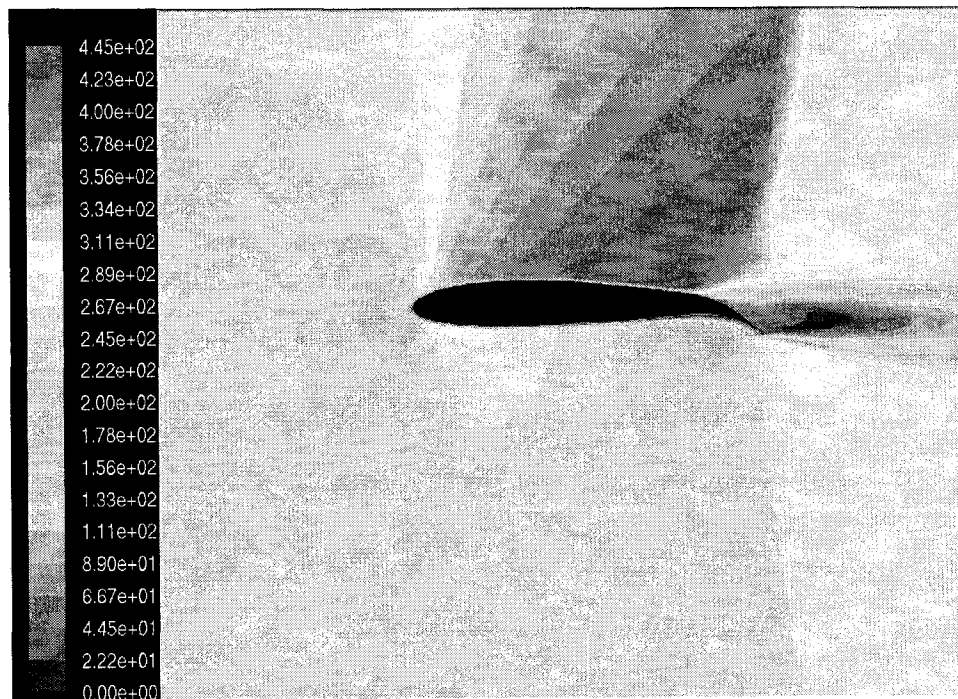


Figure 6.10 Velocity (m/s) contours at $\alpha=0$, $\delta=5^\circ$ for a parametric smart airfoil

Table 6.5 Comparison of Lift and Drag Values at $Ma=0.8$, $\delta=15^\circ$

α (deg)	C_{Lconv}	C_{Lsmart}	%increase	C_{Dconv}	C_{Dsmart}	%increase
0°	1.355	1.19	12.2	0.2218	0.1845	20.21
5°	1.69	1.57	7.64	0.35	0.31	12.9
10°	1.65	1.625	2.5	0.44	0.42	4.8
15°	1.5	1.475	1.7	0.54	0.52	2

Though there is very good improvement in lift values comparing to the bending beam method there is considerable amount of increase in drag values. Generally the flights takeoff at $M=0.22$ (see Chapter 2). Now with the new speed the simulations are done again. Two cases were analyzed here. 5 degree flap deflection angle and 15 degree flap deflection angle. Pivot point used while designing the airfoil is 0.75 m from the leading edge. The results are tabulated below.

Table 6.6 Comparison of Lift and Drag Values at $Ma=0.22$, $\delta=5^\circ$

α (deg)	C_{Lconv}	C_{Lsmart}	%increase	C_{Dconv}	C_{Dsmart}	%increase
0°	0.4364	0.4133	-5	0.0037	0.0045	21.62
5°	0.8560	0.8642	0.9	0.0207	0.0140	-32.36
10°	0.8175	0.7850	-3.9	0.1100	0.1115	1.363

For 5 degree flap deflection angle and 0 degree angle of attack, there is a reduction in lift and increase in drag. At 5 deg angle of attack, not only there is increase in lift but at the same time the drag is reduced, which is most desirable. At 10 deg angle of attack

again the lift falls down. For flap deflection angle of 15 degrees the values are tabulated below.

Table 6.7 Comparison of Lift and Drag Values at $Ma=0.22$, $\delta= 15^\circ$

$\alpha(\text{deg})$	$C_{L\text{conv}}$	$C_{L\text{smart}}$	%increase	$C_{D\text{conv}}$	$C_{D\text{smart}}$	%increase
0°	0.9378	1.304	39.1	0.021	0.0242	15.23
5°	1.181	1.398	18.371	0.0558	0.0656	17.5
10°	1.0275	1.45	41.12	0.191	0.224	3.3
15°	1.044	1.155	10.63	0.324	0.364	12.34

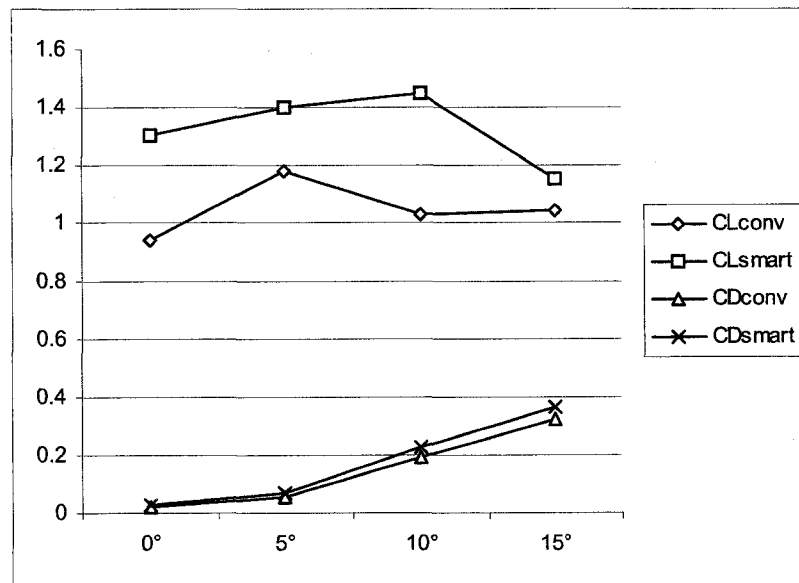


Figure 6.11 Plot between Angle of attack and coefficients of lift, drag at $\delta= 15^\circ$, $Ma= 0.22$

For 15 deg flap angle until it reaches angle of attack 15 deg the results are reasonable good but above 15 deg angle of attack the lift starts going down. The most desirable position at 15 deg flap angle is 10 –deg- angle of attack where the increase in lift is 41.12% where the increase in drag is only 3.3%.

6.3 Benchmarking Problem

NACA 66215-216 airfoil is used to benchmark our problem. All the analysis involved in this project, assumed a conventional airfoil to have a flap which has a straight-lined profile connected to the trailing edge. The reason for choosing this as a benchmarking problem is because it discusses about the lift characteristics for a plain flap (which is of sealed type and is similar to our parametric conventional airfoil) for various deflection angles. Figure 6.11 represents the experimental lift characteristic data[1] for NACA 66215-216 airfoil, plotted against the angle of attack, for different flap deflection angles, ranging from 5 degrees to -15 degrees with 5 degree increments. Since we have already discussed how the mesh files are created, this session will just give an overview and proceed to the results. Figure 6.12 shows the mesh file for 0 degree flap deflection angle.

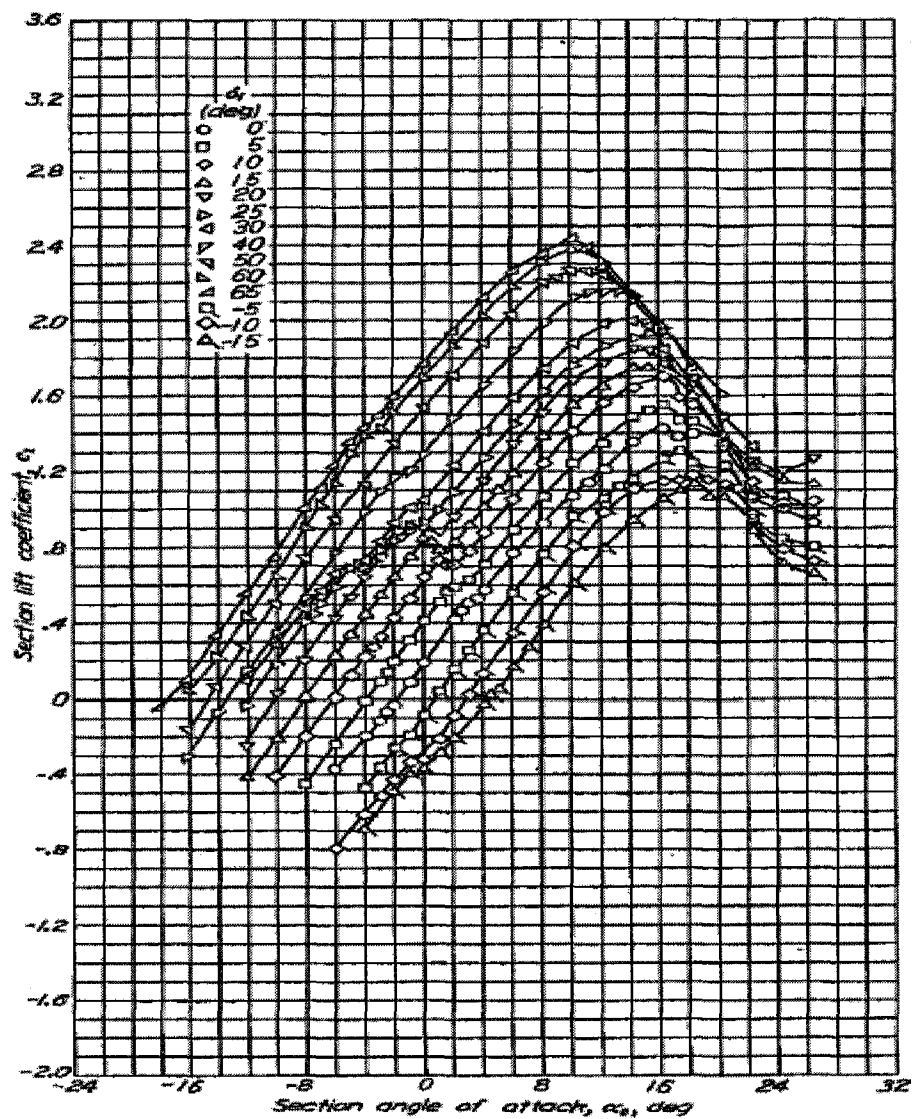


Figure 6.12 Lift characteristics of NACA 66215-216 airfoil with sealed flap

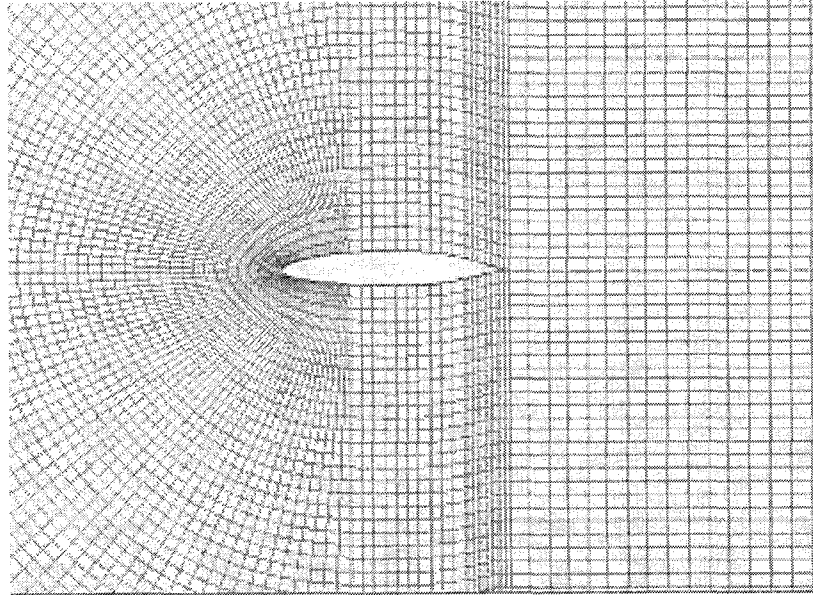


Figure 6.13 Meshed model of NACA 66215-216 airfoil

Reynolds numbers for this experiment is found to be, $Re = 6 \times 10^6$

The Mach number is found as explained below,

$$R_e = \frac{\rho V_\infty l}{\mu} \quad (6.1)$$

Therefore

$$V_\infty = \frac{R_e \mu}{\rho} \quad (6.2)$$

From air properties table,

$$\mu = 1.796674 \times 10^{-5} \text{ kg/ m .s}$$

$$\rho = 1.177 \text{ kg/ m}^3$$

By substituting the values in the equation 6.2, we get $V_\infty = 91.2 \text{ m/s}$

Since $Ma = \frac{V_{\infty}}{a}$ (6.3)

where, $a = 340$ m/s at standard sea level temperature(288K)

Substituting the value in equation 6.3, the Mach number is found to be $Ma = 0.268$

With all the boundary conditions in hand the mesh file is exported to FLUENT and solved. Figure 6.13 shows the pressure contours at zero degree angle of attack and Table 6.8 shows the values coefficients of lift for different angles of attack. Also the percentage difference between the experimental data and simulation data is tabulated.

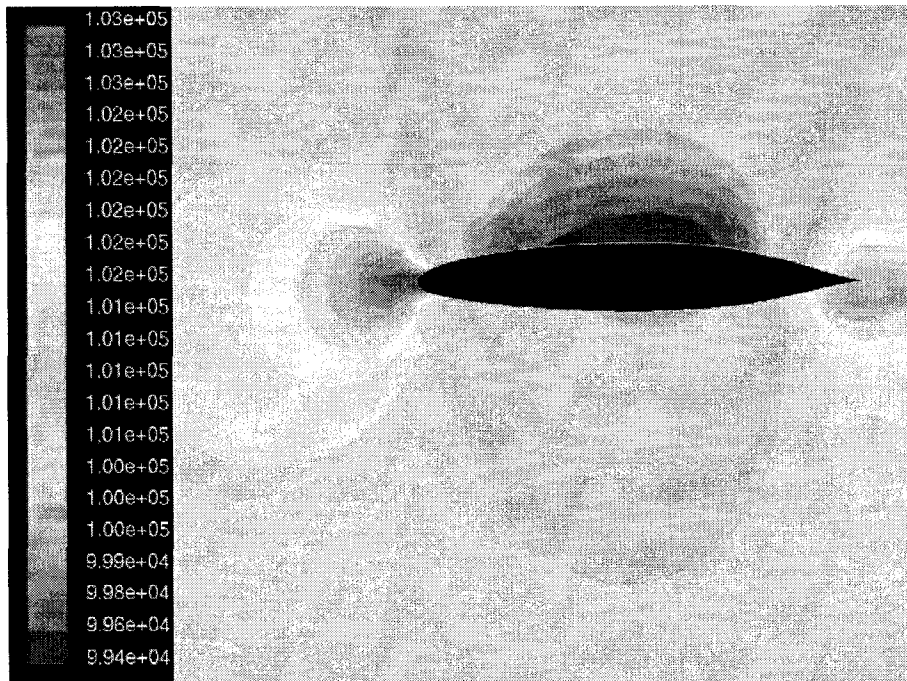


Figure 6.14 Pressure (Pa) contours ($\delta = 0^\circ$, $\alpha = 0^\circ$)

Table 6.8 Comparison between $C_{L[1]}$ and $C_{L\text{simulation}} (\delta=0^\circ)$

α (deg)	$C_{L[1]}$	$C_{L\text{simulation}}$	% difference
0°	0.2	0.155	20
4°	0.49	0.45	8.16
10	1.1	0.8	27.27
16	1.3	1.19	8.46

Even though there is a huge variation of the simulation results with the experimental data for $\delta=0$, reasonable results are obtained for flap deflection angle $\delta=5^\circ$ and $\delta=10^\circ$. The mesh file for $\delta=5^\circ$ and the tabulation of the lift characteristic data are given below. Pressure contours for different angle of attacks are shown in Figures 6.15 and 6.16

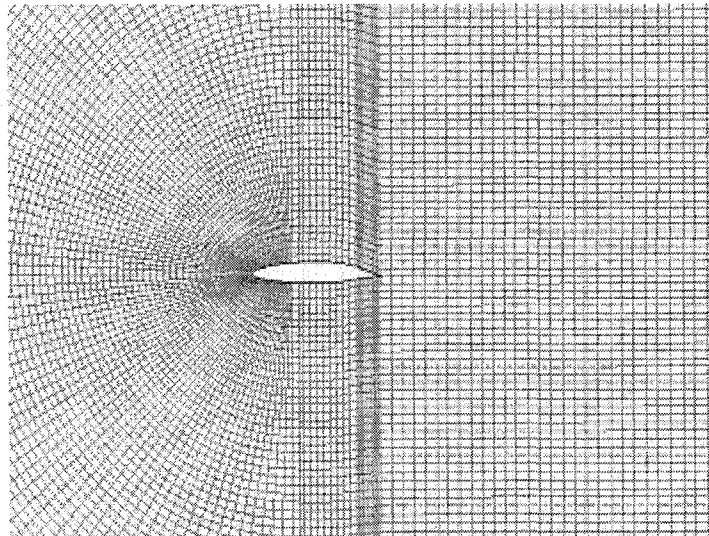


Figure 6.15 Meshed model for $\delta=5^\circ$

Table 6.9 Comparison between $C_{L[1]}$ and $C_{Lsimulation}$ ($\delta=5^\circ$)

α (deg)	$C_{L[1]}$	$C_{Lsimulation}$	% difference
0°	0.4	0.382	4.5
4°	0.68	0.62	8.82
10	0.95	0.7	26
16	1.5	1.2	20

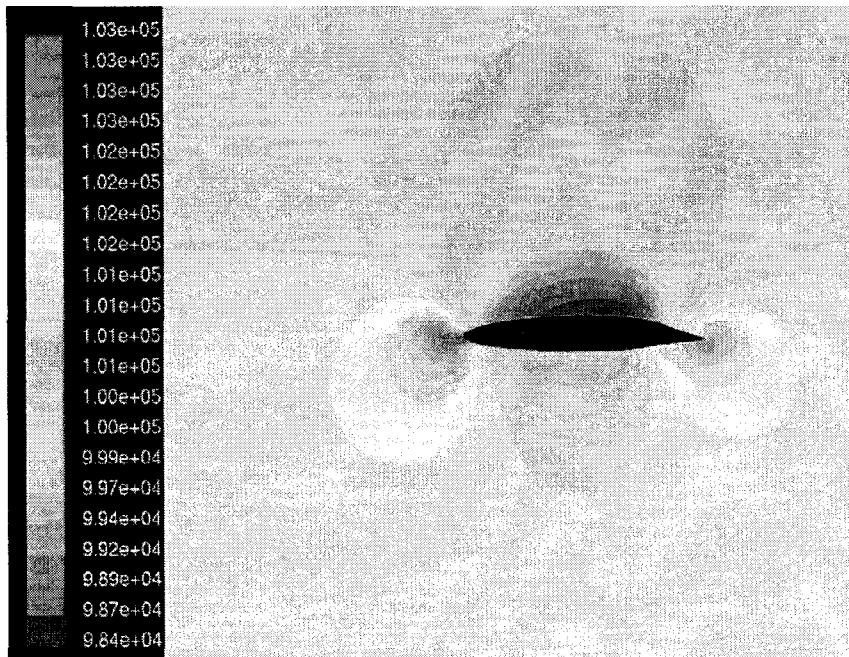


Figure 6.16 Pressure (Pa) contours at $\alpha=4^\circ$, $\delta=5^\circ$

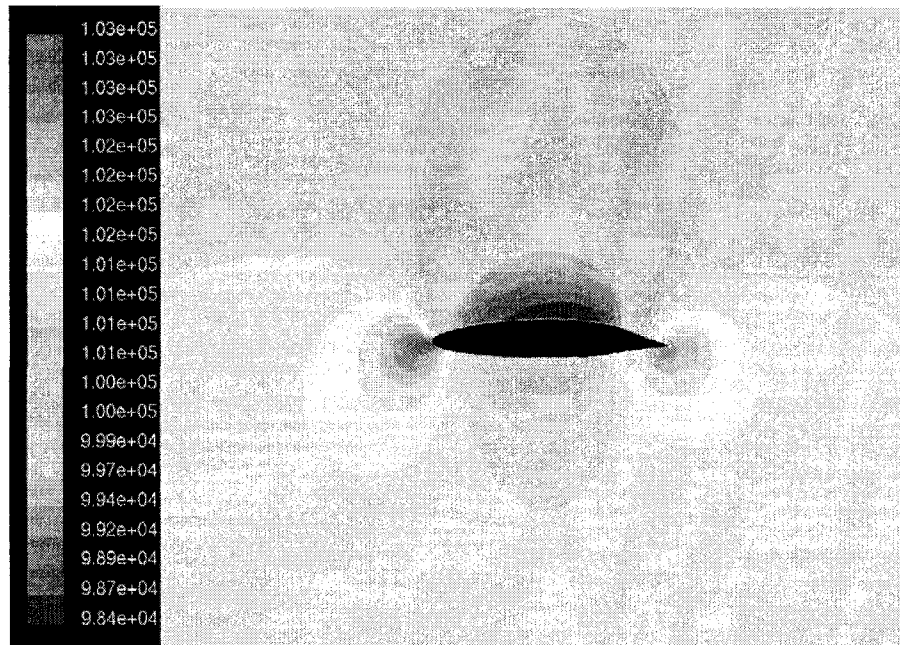


Figure 6.17 Pressure (Pa) contours at $\alpha=10^\circ$, $\delta=5^\circ$

Similarly for 15 degree flap deflection angle, the mesh file is shown in Figure 6.17 and the results are tabulated in Table 6.10.

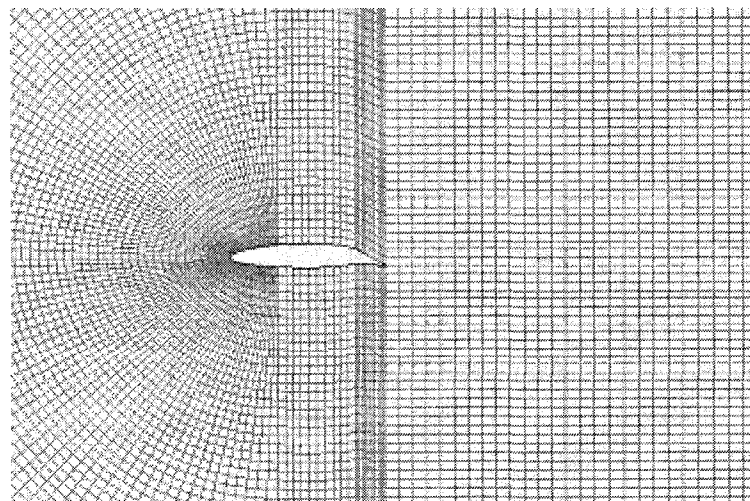


Figure 6.18 Meshed model for $\delta=15^\circ$

Table 6.10 Comparison between $C_{L[1]}$, $C_{Lsimulation}(\delta=15^\circ)$

α (deg)	$C_{L[1]}$	$C_{Lsimulation}$	% difference
0°	0.83	0.824	0.722
4°	0.99	0.93	6.06
10	1.55	1.2	22.5
16	1.7	1.5	11.76

The pressure contours for different angle of attack α is given below.

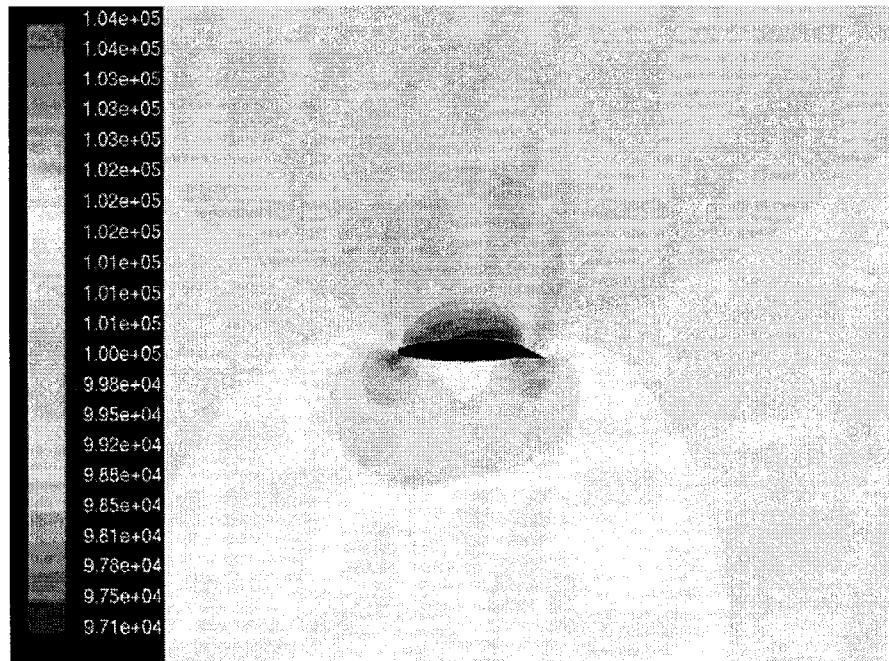


Figure 6.19 Pressure (Pa) contours at $\alpha=0^\circ$, $\delta=15^\circ$

It can be seen from the pressure contours that the low pressure area above the airfoil keeps increasing when the angle of attack is increased, thereby increasing the lift force.

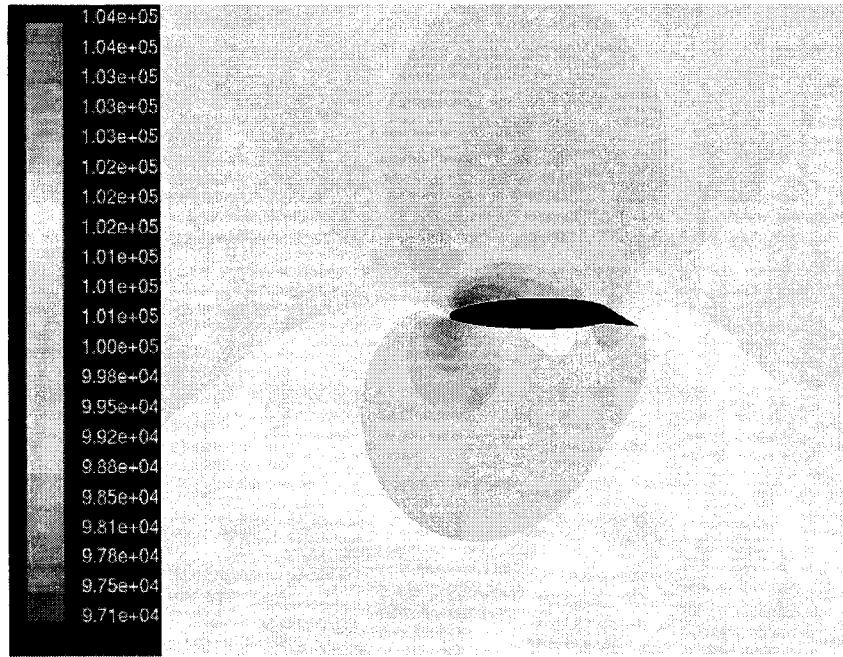


Figure 6.20 Pressure (Pa) contours at $\alpha = 4^\circ$, $\delta = 15^\circ$

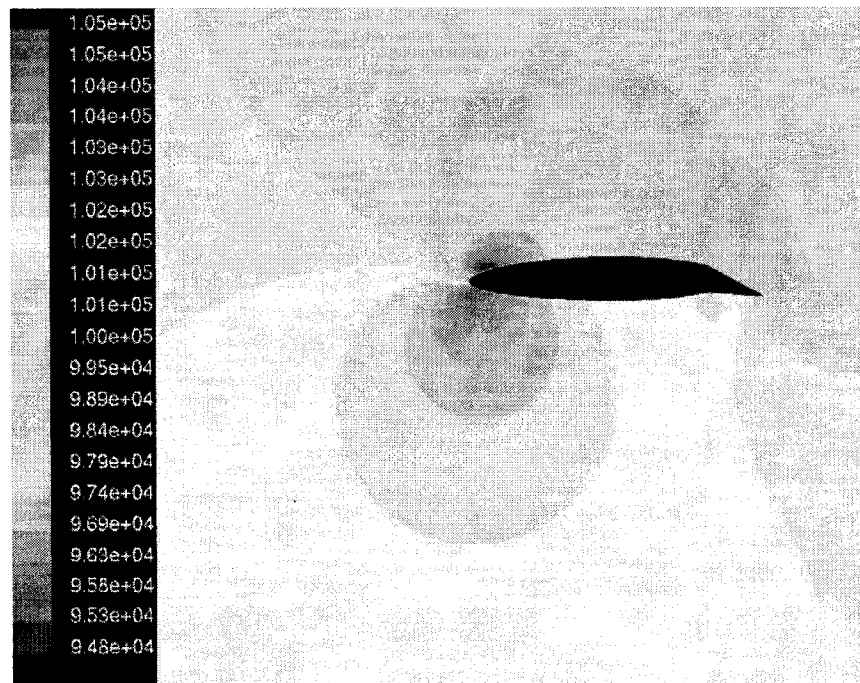


Figure 6.21 Pressure (Pa) contours at $\alpha = 10^\circ$, $\delta = 15^\circ$

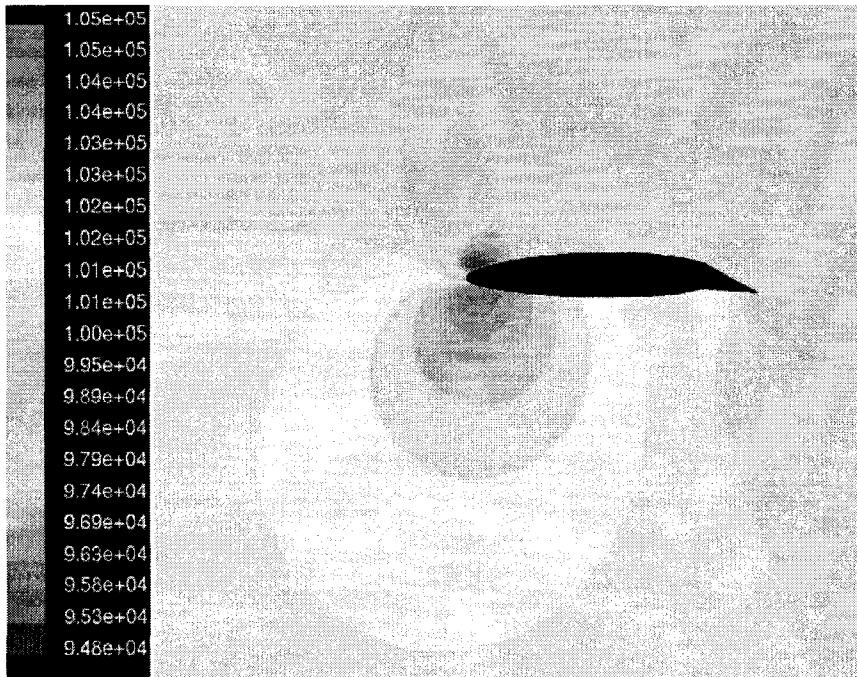


Figure 6.22 Pressure (Pa) contours at $\alpha = 16^\circ$, $\delta = 15^\circ$

6.4 Validation

It has been assumed that the trailing edge of the parametric conventional airfoil has flaps with straight lined edges and is connected with the airfoil. The simulation results were discussed in the previous section. There is a considerable variation between the experimental values and the values obtained from the simulations. The computational fluid dynamic result doesn't always agree exactly with the practical values that we get in the experiments. Calculations also show that the standard turbulence model used in most commercial CFD codes is not appropriate at angles of attack with flow separation [10]. From reference [10] we can find the following table which talks about the percentage deviation of computational fluid dynamic results from the experimental values. For

example from Table 6.11 the CFD lift coefficient can be found to be 10% less than that of the experimental one.

Table 6.11 Comparisons between calculated and experimental aerodynamic coefficients, fully turbulent conditions [19]

α deg	C_l				C_d				C_m			
	calc	exp	error $\times 10^4$	% error	calc	exp	error $\times 10^4$	% error	calc	exp	error $\times 10^4$	% error
0	0.1324	0.1469	-145	-10	0.0108	0.0070	38	54	-0.0400	-0.0443	43	-10
1.02	0.2494	0.2716	-222	-8	0.0110	0.0072	38	53	-0.0426	-0.0491	65	-13
5.13	0.7123	0.7609	-486	-6	0.0124	0.0070	54	77	-0.0513	-0.0609	96	-16

In our case (from Tables 6.9 and 6.10) we have only 4.5% (for $\delta=5^\circ$) and 0.722% (for $\delta=15^\circ$) deviation from the experimental data. Same can be seen for the all other cases. Hence the assumption made for the conventional airfoil is validated.

6.5. Effect of Changing Pivot Points

For this analysis BAC XXX airfoil is taken into consideration and the results are analyzed. The pivot points are changed and airfoils were designed for each case separately. The following three pivot points were selected. 0.75 C, 0.8 C and 0.85 C. The letter "C" denotes the chord of an airfoil. For each pivot point the mesh files were designed for three different flap deflection angles ($\delta=5^\circ, 15^\circ$ for take off conditions and -10° for landing condition). The mesh files are created as explained in Chapter 3. The results are tabulated below.

Table 6.12 Lift and drag characteristics at 0.85C, $\delta=5^\circ$

$\alpha(\text{deg})$	$C_{L\text{conv}}$	$C_{L\text{smart}}$	%increase	$C_{D\text{conv}}$	$C_{D\text{smart}}$	%increase
0°	0.4077	0.4829	18.45	0.002	0.0024	20
5°	0.7816	0.8382	7.24	0.0263	0.0296	12.54
10°	0.8623	0.8762	1.612	0.0761	0.0776	1.97
15°	0.8025	0.8232	2.57	0.1568	0.1621	3.38

Table 6.13 Lift and drag characteristics at 0.85C, $\delta=15^\circ$

$\alpha(\text{deg})$	$C_{L\text{conv}}$	$C_{L\text{smart}}$	%increase	$C_{D\text{conv}}$	$C_{D\text{smart}}$	%increase
0°	0.8288	1.0117	22	0.0107	0.0154	43.93
5°	1.0790	1.1944	10.69	0.0486	0.0588	20.99
10°	1.0046	1.0745	6.96	0.1063	0.1216	14.39
15°	0.9565	1.0256	7.224	0.2111	0.2344	11.04

Table 6.14 Lift and drag characteristics at 0.85C, $\delta= -10^\circ$

$\alpha(\text{deg})$	$C_{L\text{conv}}$	$C_{L\text{smart}}$	%increase	$C_{D\text{conv}}$	$C_{D\text{smart}}$	%increase
0°	-0.2644	-0.3555	34	0.0088	0.0113	28
5°	0.1897	0.0931	-50	0.0236	0.0564	138
10°	0.5432	0.4763	-12.3	0.0382	0.0322	-15.7
15°	0.5372	0.5079	-5.45	0.0880	0.0830	-5.68

Table 6.15 Lift and drag characteristics at $0.75C$, $\delta=5^\circ$

α (deg)	C_{Lconv}	C_{Lsmart}	%increase	C_{Dconv}	C_{Dsmart}	%increase
0°	0.4494	0.6191	37.76	0.00006	0.0001	66.7
5°	0.8195	0.9442	15.21	0.0245	0.0320	30.61
10°	0.9181	0.9556	4.08	0.0810	0.0853	5.3
15°	0.8294	0.8741	5.39	0.1596	0.1711	7.20

Table 6.16 Lift and drag characteristics at $0.75C$, $\delta=15^\circ$

α (deg)	C_{Lconv}	C_{Lsmart}	%increase	C_{Dconv}	C_{Dsmart}	%increase
0°	0.9664	1.2264	26.90	0.0137	0.0224	63.50
5°	1.172	1.3344	13.85	0.0585	0.0751	28.37
10°	1.0846	1.3144	21.187	0.1248	0.1910	54.03
15°	1.0162	1.1114	9.36	0.2372	0.2705	14.03

Table 6.17 Lift and drag characteristics at $0.75C$, $\delta=-10^\circ$

α (deg)	C_{Lconv}	C_{Lsmart}	%increase	C_{Dconv}	C_{Dsmart}	%increase
0°	-0.4196	-0.5409	28.9	0.0118	0.0158	33
5°	-0.0353	-0.0947	168	-0.0028	-0.0047	67
10°	0.4294	0.3299	-23	0.0242	0.0173	-28
15°	0.5708	0.5092	-10.8	0.0858	0.0761	-11.3

Table 6.18 Lift and drag characteristics at 0.80C, $\delta=5^\circ$

α (deg)	C_{Lconv}	C_{Lsmart}	%increase	C_{Dconv}	C_{Dsmart}	%increase
0°	0.5952	0.8866	48.95	0.0168	0.0202	20
5°	0.8782	1.0919	24.33	0.0577	0.0668	19.23
10°	0.8270	1.0088	21.98	0.1088	0.1275	17.18
15°	0.8280	0.9626	16.26	0.2288	0.1089	52.4

Table 6.19 Lift and drag characteristics at 0.80C, $\delta=15^\circ$

α (deg)	C_{Lconv}	C_{Lsmart}	%increase	C_{Dconv}	C_{Dsmart}	%increase
0°	0.8952	1.1083	23	0.0151	0.0149	-1.34
5°	1.1258	1.274	13.16	0.0600	0.0651	8.5
10°	1.0244	1.1389	11.17	0.1144	0.1322	15.55
15°	0.9830	1.0724	9.1	0.2208	0.2492	12.86

Table 6.20 Lift and drag characteristics at 0.80C, $\delta= -10^\circ$

α (deg)	C_{Lconv}	C_{Lsmart}	%increase	C_{Dconv}	C_{Dsmart}	%increase
0°	-0.3377	-0.4457	31.98	0.0105	0.0138	31.42
5°	0.1044	-0.0092	108	0.0016	-0.0008	150
10°	0.4755	0.3949	-16.9	0.0344	0.0282	-18.02
15°	0.5857	0.5384	-8.1	0.0960	0.0877	-8.6

From the results it can be seen that the 0.8 pivot point smart wing gives better performance than the other two. It can be seen drag is increased almost twice the amount of lift for 0.75 and 0.85 cases. Though these results may not be generalized for all the airfoils it holds good for BAC XXX airfoils. The bench marking problem discussed in the previous section was three-dimensional one. This study was only focused on two-dimensional performance characteristics. Naturally the results might vary in a real world situation. The future work can be focused on three-dimensional smart wings.

CHAPTER 7

CONCLUSION AND SUGGESTIONS

The computational fluid dynamics models of the flexible airfoils were analyzed in this study and optimum values of lift and drag coefficients were obtained for various angles of attack and flap deflection angles. Software tools like MATLAB, SOLIDWORKS were used to obtain data files of the bending airfoil. GAMBIT was used to obtain the computational mesh and FLUENT was used to solve the problem. Bending beam method and tangent arc method were the two methods used to design the smart airfoil in this study. The most desirable position of NACA 1412 smart airfoil at 15 deg flap angle was when $\alpha=10^\circ$, where the increase in lift is 41.12% but the increase in drag is only 3.3% comparing to the parametric conventional airfoil ($Ma=0.22$). At $\delta=5^\circ$, $Ma=0.22$ and $\alpha=5^\circ$ (for NACA 1412) the lift increases while the drag reduces comparing to the conventional airfoil, which is most desired. The values of lift and drag coefficients obtained from the CFD simulations were then compared with the experimental data to validate the assumption made for the conventional airfoil. NACA 66215-216 airfoil is used to validate the assumption made for the conventional airfoil. $Ma=0.268$. The simulation results had reasonable variation with the experimental results. One of the main reasons for the variation is the model under investigation is a two-dimensional model, where as the experimental model is three-dimensional one.

The flexible wing can also be designed in several other ways based on the bending profile that is selected. Each method has a unique design, where one gets optimum aerodynamic characteristics.

In future with the aid of advanced technologies in controls engineering, the best profiles obtained in each method can be collected and selected instantaneously based on our needs. The smart material would then take the shape of the profile which has just been assigned. This work can further be extended to the study of computational fluid dynamics on a three-dimensional smart wing design.

REFERENCES

- [1] Ira H. Abbot, Theory of wing sections including summary of Airfoil data, 1959, Dover Publications, New York.
- [2] Anand Natarajan, Aero elasticity of morphing wings using neural networks, Ph. D. Dissertation, Virginia tech, Blacksburg, Virginia, July 2002.
- [3] George Akhras, smart materials and smart systems for the future, Canadian Military Journal, autumn 2000.
- [4] Anderson, Fundamentals of aerodynamics, 2001, Mc-Graw Hill, 3rd edition.
- [5] Ed Stern stein and Todd Gold, From takeoff to landing, 1991 Pocket Books, New York.
- [6] Daniel, T.L. and Combes, S.A. (2002), Flexible wings and fins: bending by inertial or fluid Dynamic Forces Int.Comp. Biol. 42(5), pp. 1044-1049.
- [7] H. Sobieczky, W. Geisseler, and M. Hannemann (1997), Numerical tool for unsteady viscous flow control, Proc. 15th Int. Conf. on Num. Meth. in Fluid dynamics. Lecture notes in physics, ed. P. Kutler, J. Flores, J. J. Chattot, Springer (Berlin, Heidelberg).
- [8] Helmut Sobieczky (1998), Parametric airfoils and wings, in: Notes on numerical Fluid Mechanics, pp. 71-88, Vieweg Verlag.
- [9] Jacob, J.D., On the fluid Dynamics of adaptive airfoils, ASME International Mechanical Engineering Congress and Exposition, Nov. 15-20, 1998, Anaheim, CA. planned to defend.

- [10] Garg D.P., Zirkry M.A. and Anderson G.L., Current and future research activities in adaptive structures: an ARO perspective, Journal of Smart materials and structures, Vol.10 (4): 2001, pp.610-623.
- [11] Kornbluh, R., R. Pelrine, Q. Pei, S. Oh, and J. Joseph, Ultrahigh strain response of field actuated elastomeric polymers, Proceedings of SPIE Smart materials April 2000.
- [12] Ramakrishnananda, B. and Wong, K. C., Animating bird flight using aerodynamics, The Visual Computer, Vol. 15 (10), 1999, pp. 494-508.
- [13] Rathnasingam, R. system identification and active control of turbulent boundary layer, Ph. D. Thesis, Dept. of Aeronautics and Astronautics, MIT, May 1997.
- [14] Jameson A. And Vassberg, J. C., computational fluid dynamics for aerodynamic design-Its current and future impact, paper 2001-0538, 39th AIAA Aerospace Sciences Meeting and Exhibit, Reno, Jan 8-11, 2001.
- [15] Trease, B. P., Lu, K. J., Kota .S, Biomimetic compliant system for smart actuator-driven aquatic propulsion: preliminary results, 2003, proceedings of IMECE
- [16] Ira H. Abbott, Albert E. von Doenhoff, and Louis S. Stivers,Jr., “ Summary of Airfoil data”,NACA Rept No.824, 1945
- [17] Parthasarathy Chinnasamy and Yitung Chen , Computational fluid dynamics on smart wing design, 43rd AIAA Aerospace Sciences Meeting and Exhibit, Reno, NV10-13 Jan 2005.
- [18] Carl J. Wenzinger and Fransis M. Rogallo, Resume of air load data on slats and flaps ,NACA Rept. No. 690, 1939.

- [19] Walter P. Wolfe and Stuart S. Ochs, CFD Calculations of S809 Aerodynamic Characteristics, AIAA-97-0973.
- [20] Pinkerton, J. L. and Moses, R. W., “A feasibility study to control airfoil shape using THINDER” NASA TM 4767, Nov.1997
- [21] Carl J. Wenzinger, Wind-tunnel investigation of ordinary and split flaps on airfoils of different profile, NACA Rept No. 554, 1936
- [22] Ferdinand P. Beer, E. Russell Johnston, Jr., John T. DeWolf, Mechanics of Materials, 4th Edition, McGraw-Hill, 2002.

VITA

Graduate College
University of Nevada, Las Vegas

Parthasarathy Chinnasamy

Local Address:

4210 Fairfax Circle, Apt#01
Las Vegas, NV 89119

Degree:

Bachelor of Engineering
Mechanical Engineering, 2002
SSM College of Engineering, Periyar University, Tamil Nadu, India.

Special Honors and Awards

Recipient of "NASA EPSCoR student travel grant" for the year 2004
Best outgoing student award of the year 2001-2002, S.S.M. College of
Engineering, INDIA

Presentations:

Parthasarathy Chinnasamy and Yitung Chen "Computational fluid dynamics
on smart wing design", 43rd AIAA Aerospace Sciences Meeting and
Exhibit, Reno, NV, 10-13, Jan 2005.

Thesis Title:

Computational Fluid Dynamics on Smart Wing Design

Thesis Examination Committee:

Chairperson, Dr. Yitung Chen, Ph.D.
Committee Member, Dr. William Culbreth, Ph.D.
Committee Member, Dr. Woosoon Yim, Ph.D.
Graduate Faculty Representative, Dr. Shajendra Singh, Ph.D.